SYNTHESIS AND CHARACTERIZATION OF MONTICELLITE ($CaMgSiO_4$) BASED BIOACTIVE CERAMIC POWDERS OBTAINED FROM BORON DERIVATIVE WASTE

Master of Science Thesis

Levent KÖROĞLU
Eskişehir, 2018

SYNTHESIS AND CHARACTERIZATION OF MONTICELLITE ($CaMgSiO_4$) BASED BIOACTIVE CERAMIC POWDERS OBTAINED FROM BORON DERIVATIVE WASTE

Levent KÖROĞLU

MASTER OF SCIENCE THESIS

Graduate School of Sciences
Material Science and Engineering Program
Supervisor: Assoc. Prof. Dr. Erhan AYAS

Eskişehir
Anadolu University
Graduate School of Science
January, 2018

This thesis work is supported by the Scientific Research Projects Commission of Anadolu University [grant number: 1607F584] and by the Scientific Research Projects Commission of The Scientific and Technological Research Council of Turkey (TÜBİTAK) [grant number: 116M218].

FINAL APPROVAL FOR THESIS

This thesis titled "Synthesis and Characterization of Monticellite ($CaMgSiO_4$) Based Bioactive Ceramic Powders Obtained from Boron Derivative Waste" has been prepared and submitted by Levent KÖROĞLU in partial fullfillment of the requirements in "Anadolu University Directive on Graduate Education and Examination" for the Degree of Master of Science in Materials Science and Engineering Department has been examined and approved on 05/01/2018.

	Committee Members	Signature
Member (Supervisor) :	Assoc. Prof. Dr. Erhan AYAS	…….
Member :	Prof. Dr. Ayşe Tansu KOPARAL	……..
Member :	Assist. Prof. Dr. Ceren PEKŞEN	…….....

……

Director

Graduate School of Science

ABSTRACT

Synthesis and Characterization of Monticellite ($CaMgSiO_4$)
Based Bioactive Ceramic Powders Obtained from Boron Derivative Waste

Levent KÖROĞLU

Department of Materials Science and Engineering
Anadolu University, Graduate School of Science, January 2018
Supervisor: Assoc. Prof. Dr. Erhan AYAS

In this thesis, the presenting of a novel approach in a cost-effective and environmentally friendly way for the synthesis of monticellite based bioactive ceramic powders from boron derivative waste was intended. The aims of the study are the solid-state synthesis of monticellite based ceramic powders from boron derivative waste, the investigation of the effect of particle size on bone-like apatite formation ability of monticellite based ceramic powders and the determination of the cytotoxicity of monticellite based ceramic powder. Also, the phase transformation mechanism of boron derivative waste was investigated during systematic heat-treatments and monticellite phase could be formed at 650°C. The most stable monticellite based ceramic powder was synthesized at 800°C for 4 h (SP-800°C-4h) and its ball-milling time was optimized. Following to immersion of wafers composed of crushed SP-800°C-4h and ball-milled SP-800°C-4h for 2 h in Lac-SBF for 7 days, the obtained results showed that monticellite based ceramic powders have bone-like apatite formation ability and it is improved by the particle size reduction. The cytotoxicity of monticellite based ceramic powder, comprising monticellite, akermanite, diopside and calcium magnesium borate phases, on different mammalian cell lines (3T3-L1, HUVEC, CRL-2120) was determined by *in vitro* assays of MTT, NRU and JC-1 staining at the concentrations of 10, 50, 100, 200, 400, 500 and 800 μg/ mL. The results indicated the biocompatible characteristic of monticellite based ceramic powder at the concentration range of 10 - 200 μg/ mL.

Keywords: Monticellite ($CaMgSiO_4$), Bioactive Ceramics, Solid-State Powder Synthesis, Boron Derivative Waste, *In Vitro* Tests

ÖZET

Bor Türev Atığından Montiselit ($CaMgSiO_4$) Esaslı
Biyoaktif Seramik Tozların Sentezi ve Karakterizasyonu

Levent KÖROĞLU

Malzeme Bilimi ve Mühendisliği Anabilim Dalı
Anadolu Üniversitesi, Fen Bilimleri Enstitüsü, Ocak 2018
Danışman: Doç. Dr. Erhan AYAS

Bu tez çalışmasında, ekonomik ve çevreci bir yöntem ile bor türev atığından montiselit esaslı biyoaktif seramik tozlarının sentezlenmesi adına yeni bir yaklaşım sunmak istenmiştir. Bor türev atığından montiselit esaslı seramik tozların katı-hal sentezi, sentezlenen tozların tane boyutunun kemik-benzeri apatit oluşumu üzerine etkilerinin araştırılması ve montiselit esaslı seramik tozların sitotoksisitesinin incelenmesi bu çalışmanın amaçlarını oluşturmaktadır. Bununla birlikte sistematik ısıl işlemler eşliğinde atığın faz dönüşüm mekanizması araştırılmıştır ve montiselit fazı 650°C'de elde edilmiştir. En kararlı montiselit esaslı seramik tozu 800°C'de 4 saat süresince sentezlenmiştir ve bu tozu (SP-800°C-4h) öğütme süresi bilyalı değirmen kullanılarak optimize edilmiştir. Kırılmış ve 2 saat süresince öğütülmüş tozlardan oluşan peletlerin Lac-SBF içerisinde 7 gün bekletilmesinin ardından elde edilen sonuçlar, montiselit esaslı seramik tozların kemik-benzeri apatit oluşumunu sağladığını ve tane boyutun azalması ile bu oluşumun hızlandığını göstermektedir. Montiselit, akermanit, diopsit ve kalsiyum magnezyum borat fazlarından oluşan montiselit esaslı seramik tozun farklı memeli hücreleri (3T3-L1, HUVEC, CRL-2120) üzerindeki sitotoksisitesi *in vitro* MTT, NRU ve JC-1 renklendirme testleri ile farklı konsantrasyonlarda (10, 50, 100, 200, 400, 500, 800 µg/ mL) değerlendirilmiştir. Sonuçlar, montiselit esaslı seramik tozun 10 - 200 µg/ mL konsantrasyon aralığında biyouyumlu olduğuna işaret etmektedir.

Anahtar Sözcükler: Montiselit ($CaMgSiO_4$), Biyoaktif Seramikler, Katı-Hal Toz Sentezi, Bor Türev Atığı, *In Vitro* Testler

ACKNOWLEDGMENTS

I would like to take this opportunity to express my sincere gratitude to my supervisor, Assoc. Prof. Dr. Erhan AYAS due to his endeavors and patience throughout my thesis work. In addition, his sincerity and guidance on all issues make him more than a supervisor.

I wish to thank Prof. Dr. Ayşe Tansu KOPARAL (Department of Biology, Anadolu University) and Assist. Prof. Dr. Ceren PEKŞEN (Department of Ceramic and Glass, Ondokuz Mayıs University) who give an opportunity to collaborate work, for their contributions and valuable advices.

I would like to thank Aslı Asiye AĞIL, Berkay YAZIRLI, İrem KAĞNICIOĞLU, Kübra GÜRCAN, Levent KARACASULU, Meriç Çetin GÜVENÇ and Tuğçe Aybüke ARICA for their supportive friendship. Also, I am thankful to Merve TANER who always gives me their moral and material support.

I am eternally grateful to my parents (Fikret KÖROĞLU & Güler KÖROĞLU) and my sister (Serra KÖROĞLU) for their constant and endless supports, words cannot express my gratitude.

Levent KÖROĞLU

Eskişehir, 2018

16/01/2018

STATEMENT OF COMPLIANCE WITH ETHICAL PRINCIPLES AND RULES

I hereby truthfully declare that this thesis is an original work prepared by me; that I have behaved in accordance with the scientific ethical principles and rules throughout the stages of preparation, data collection, analysis and presentation of my work; that I have cited the sources of all the data and information that could be obtained within the scope of this study, and included these sources in the references section; and that this study has been scanned for plagiarism with "scientific plagiarism detection program" used by Anadolu University, and that "it does not have any plagiarism" whatsoever. I also declare that, if a case contrary to my declaration is detected in my work at any time, I hereby express my consent to all the ethical and legal consequences that are involved.

.....

Levent KÖROĞLU

TABLE OF CONTENTS

LIST OF TABLES

Page

LIST OF FIGURES

Page

LIST OF SYMBOLS AND ABBREVIATIONS

°	: Degree
$	: Dollar
Å	: Angstrom
Ø	: Diameter symbol
ºC	: Degree celcius
β	: Beta
Δ	: Delta
λ	: Wavelength
μ	: Micro
θ	: Theta
A.D.	: After death
atm	: Atmospheric pressure
cm	: Centimeter
d	: Diameter
FDA	: United States Food and Drug Administration
FWHM	: Half maximum intensity in radian
g	: Gram
GPa	: Gigapascal
h	: Hour(s)
ICDD	: The International Centre for Diffraction Data
JC-1	: 5,5'6,6'-tetrachloro-1,1'3,3'-tetraethylbenzimidazol carbocyanine iodide
JCPDS	: Joint Committee on Powder Diffraction Standards
Lac-SBF	: Lactated-Simulated Body Fluid
MBCPs	: Monticellite based ceramic powders
min	: Minute(s)
mm	: Millimeter
MTT	: Mitochondrial activity
nm	: Nanometer
NRU	: Neutral red uptake
ppm	: particle per mass

SBFs : Simulated body fluids

SD : Standard deviation

SPSS : Statistical Package for Social Sciences

T : Temperature

U/ mL : Units per milliliter

UN DESA : United Nations Department of Economic and Social Affairs

v/v : Volume per volume

wt. : Weight

ΔG : Delta Gibbs free energy

ΔH : Delta enthalpy

ΔS : Delta entropy

µg/ mL : Microgram per milliliter

µl : Microliter

µM : Micromolar

µm : Micrometer (micron)

1. INTRODUCTION

The world population was 7.5 billion in 2017 and it will reach to 9.7 billion by 2050 according to the United Nations Department of Economic and Social Affairs (UN DESA). Also, it is announced that the ratio of elderly population aged 65 years and over is expected to unprecedentedly rise from 8.7 % in 2017 to 15.8 % in 2050. Due to significantly high human population and elderly population, there will be a significant increase in the number of deformity and loss of bone tissue resulting from arthritis and osteoporosis. In last decades, the unavoidable increment in musculoskeletal system diseases and injuries, caused by in a number of high energy accidents (traumas) especially in developing countries, have caused to be defined the first decade of the 21st century as "Bone and Joint 10 Year" in the worldwide. The main aim of making this definition “Bone and Joint 10 Year” are to increase awareness, to encourage the patients to take decisions about treatment and care and also, to increase the number of funds to conduct more research focused on low cost treatment methods [1-4]. At this point, in order to treat musculoskeletal system diseases and injuries arising from traumas and/or diseases, the duty of biomaterials scientists and biomaterials engineers is to produce high performance biomaterials or to improve existent biomaterials in a cost-effective and environmentally friendly way.

2. BONE, BONE GRAFTS AND BONE HEALING MECHANISMS

2.1. Structure and Properties of Bone

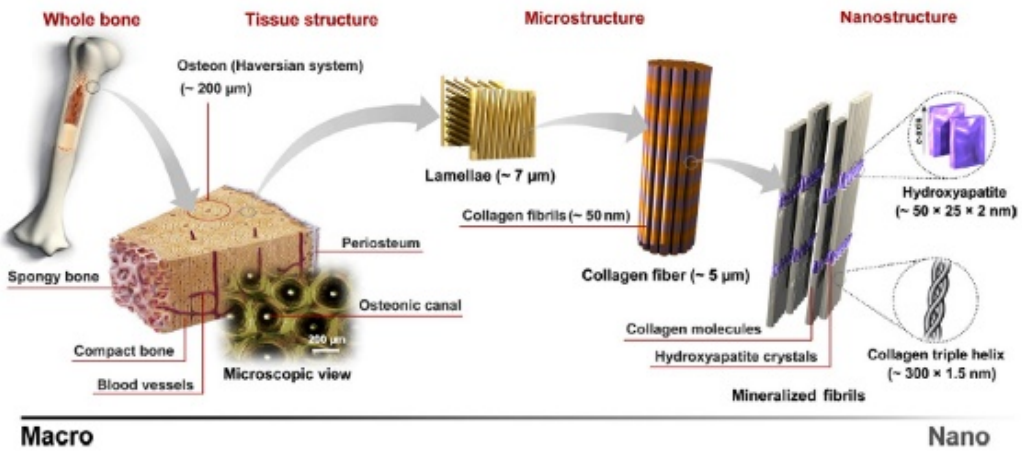

Figure 2.1. *The hierarchical structure of bone tissue*

Human bone is a composite tissue which protects the body, provides the movement along with the muscles, regenerates the blood and stem cells in marrow and storages some minerals. Bone tissue is a complex and permanently varying system. Its structure is divided into two parts as organic and inorganic architectures. The organic structure comprises mainly collagen (35 wt.%) whereas the inorganic structure is composed of bone minerals (69 wt.%) and water (9 wt.%). The rest is of non-collagenous proteins, polysaccharides and lipoids. Bone minerals are formed of hydroxyapatite (HA, $Ca_{10}(PO_4)_6(OH)_2$) and tricalcium phosphate (TCP, $Ca_3(PO_4)_2$) in 85 wt.%, calcium carbonate in 10 wt.%, calcium fluoride in 2-3 wt.% and magnesium fluoride in 2–3 wt.%. Collagen provides rigidity, viscoelasticity and toughness, minerals give stiffness and homeostasis to the bone and other proteins creates a microenvironment stimulatory to cellular functions [1, 5-6]. The hierarchical structure of bone tissue is given in Fig. 2.1 [7]. Sub-nanostructure of bone tissue includes mineral, collagen, and non-collagenous organic proteins. Collagen in the form of fibrils with a diameter range of 100 to 2000 nm and embedded HA crystals in needle shape in dimensions of averagely 50x25x2 nm construct the collagen fibers. Even if the collagen fibers are abundant in different microstructures, haversian systems and osteons built up cortical (compact) part and single trabeculae develops the trabecular (cancellous or spongy) part of the bone tissue. The structural unit of cortical bone is called osteon. Osseous cylinders create dense and hard intertwined framework where they inserted in another one. Therefore, cortical bone optimizes articular load transfer and provides high strength and fracture toughness. Also, bone tissue is covered with periosteum layer and the high number of osteoblasts located in the inner layer of periosteum. Vessels and nerves in periosteum layer allow nutrient transportation while osteoblasts are responsible for bone growth [1, 5-6].

Table 2.1. *Physical and mechanical properties of cortical and trabecular bone*

Bone	**Density (g/cm^3)**	**Porosity (%)**	**Strain (%)**	**Young Modulus (GPa)**	**Fracture Toughness ($MPa\ m^{1/2}$)**
Cortical	1.80	3-12	1-3	7-30	2-12
Trabecular	0.2	50-90	5-7	0.5-0.05	-

Physical and mechanical properties of cortical and trabecular bone are given in Table 2.1. [1, 5-6]. Trabecular bone has too low density (0.2 g/cm^3) and very high porous

matrix (50-90%) with an average trabecular spacing of around 1 mm. The interconnecting framework of rod and plate-shaped in trabeculae can absorb loads accompanied by high strain (5-7%). However, non-uniform porous matrix makes it non-possible to obtain a high value of Young modulus and fracture toughness. Unlike trabecular bone, cortical bone has an average density of 1.80 g/cm^3 due to its denser structure with a porosity of 3-12 %. Concentric cylindrical lamellar elements of osteon are roughly parallel to the long axis of the bone. For this reason, cortical bone has lower strain (1-3 %) and higher Young modulus (7-30 GPa) values than trabecular bone. Moreover, high fracture toughness (2-12 MPa.m$^{1/2}$) is obtained by this complex structure in line through fracture mechanisms of brittle-matrix composites. As a result, bone can be considered as an anisotropic material. It possesses interesting hierarchical architecture and complex cellular composition. Its mechanical properties such as Young's modulus, tensile strength and compressive strength show variability depending on many parameters such as age and disease condition of the patient, microstructure and mineralization of bone, anatomical location and especially direction of the applied load as longitudinal or transverse [1, 5-6].

2.2. Bone Grafts

The human skeleton has an outstanding ability to regenerate itself as an adult human liver. However, spontaneous bone healing in terms of shape, size and strength are not always ideal [8]. For this reason, bone grafts are widely used in order to treat skeletal fractures, or replace and regenerate lost bone tissue and or accelerate bone healing with growth factors and related agents that impart a substantial part of modern medical practice [1,2,9,10]. The field of orthopedic surgery has gained extensive experience about bone grafts over the last 20 years [8]. 2.2 million bone grafts are annually employed in worldwide during bone repair surgeries [1].

Bone grafts are classified into four groups: autografts, allografts, xenografts and bone graft substitutes. Autograft (autologous bone graft) is an osseous matter which is taken from one anatomic site of own patient and transplanted to another site. Although this type of bone grafting offers complete histocompatibility, it has plenty of limitations including limited supply, donor site pain, blood loss, high operative time, donor site infection and morbidity. Limited supply is a special challenge in pediatric patients and donor site pain is specified as the most common complication. Allograft (allopathic bone

graft) and xenograft are bone parts harvested from a human cadaver and an animal cadaver, respectively. They can be obtained from bone banks. They are transplanted to a recipient after sterilizing. The lack of donor site morbidity and decreased surgical times make them more preferable compared to autografts. For instance, over 200,000 allografts are used per year in the USA. However, they have still some restrictions such as high cost, the risk of infectious agents carried through the blood which can cause hepatitis diseases and also immune rejection. Bone graft substitutes are synthetic materials produced artificially. In comparison with autografts, allografts and xenografts, bone grafts substitutes (synthetic bone grafts) have neither morbidity problems nor risks of viral transmission. Moreover, they are cheaper and its availability is practically limitless. Bone graft substitutes can be implanted in the forms of particle or bulk solid such as powders, beads, strips and scaffolds (pellets) for the purposes of void filling, fixation and supporting of bone and coating on implants. In addition, they can be mixed with biologically active components such as antibiotics, collagens, growth factors and even mesenchymal stem cells (MSCs). Therefore, bone graft substitute is the most widely used one among bone grafts as bone-tissue repair materials and also, they have attracted growing interests for tissue engineering applications which focused on the development of osteogenic, osteoconductive and osteoinductive mechanisms [1, 8, 11].

2.3. Bone Healing Mechanisms

Bone graft substitutes provide natural bone healing through two mechanisms:

Osteoconductivity gives implanted bone graft substitutes a feature which allows bone growth on implant surface or down into pores and channels by stimulating bone cells and encouraging them to migrate into the scaffold. An interfacial surface is provided that permits bone migration by ingrowth of host capillaries, perivascular tissue and mesenchymal stem cells (MSCs). The initiation of osteoconductive bone response depends on the chemical composition and surface texture of bone graft substitute.

Osteoinductivity is a property which stimulates mesenchymal stem cells (MSCs) or mesenchymal progenitor cells to proliferate and differentiate in order to develop into osteoblasts within close proximity of bone graft substitute and newly formed bone, regardless of the site of implantation. On the concept of bone tissue engineering, bone repair and regeneration could be enhanced by incorporating of bone progenitor cells and growth factors into bone graft substitutes. Primarily used growth-factors are bone

morphogenetic proteins (BMP), platelet-derived growth factor (PDGF), interleukins, fibroblast growth factors (FGF), granulocyte-macrophage colony-stimulating factors and angiogenic factors [1,8,12].

3. BIOMATERIALS

Biomaterial is defined by The National Institute of Health Consensus Development Conference of November 1982 as "any substance (other than a drug) or combination of substances, synthetic or natural in origin, which can be used for any period of time, as a whole or as a part of a system which treats, augments, or replaces any tissue, organ, or function of the body [13]. The introduction of biomaterials into the human body has taken place for last 4000 years. To give some well-known examples for implantation throughout history, the ancient Mayans used sea shells as artificial teeth in 600 A.D. Similarly, a wrought iron was implanted for dental application in 200 A.D. in France and osseointegration was achieved. Nevertheless, early attempts for implantation of biomaterials into the body were rather hit-or-miss. In 1508, Leonardo da Vinci described the notion of contact lenses. William Harvey created an idea for replacing of heart by an artificial pump in 1628. In the early twentieth century, the interaction between body and implant started to be investigated by a number of physicians. After the first formal assessments of "biocompatibility" by Harold Ridley, he developed artificial intraocular lens made from polymethylmethacrylate. Nowadays, it is widely used to replace eye lens damaged by cataract. Moreover, bone graft substitutes, dental implants, breast implants, stents, heart valves, etc. improve the life standards of millions of people in worldwide. These biomaterials can be implanted into body systems (skeletal, muscular, nervous, endocrine, etc.) for a short period of time or a lifetime thanks to realized developments in the field of biomaterials in last years as a result of the endeavors of biomaterial scientists [14-16]. Illustrations of various implants and medical devices for human anatomy are given in Fig. 3.1 [17].

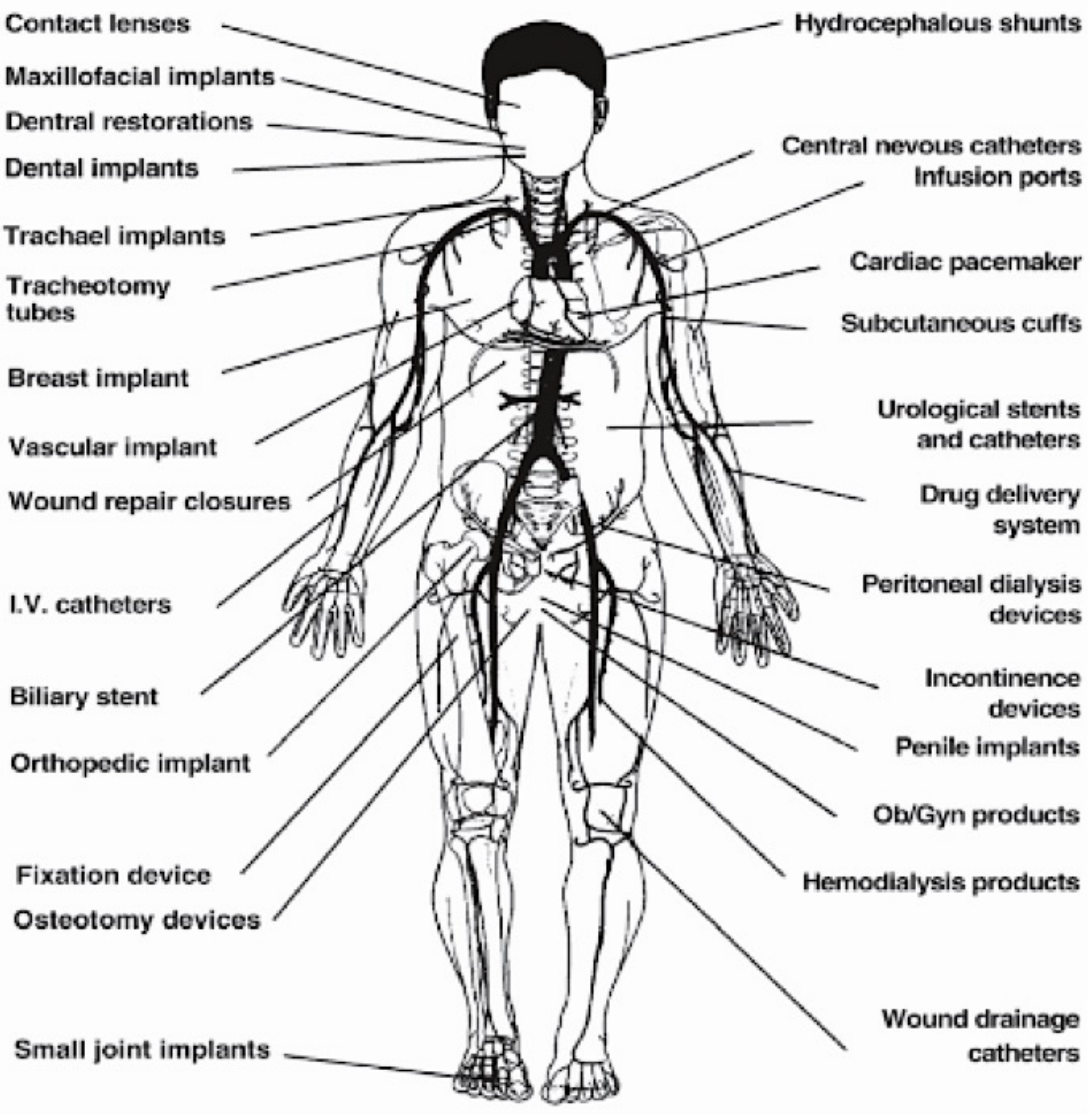

Figure 3.1. *Illustrations of various implants and medical devices for human anatomy*

Manufacturer companies have to get an approval from related administrations to show biomaterials up in the market before the usage. According to United States Food and Drug Administration (FDA), new developed biomaterials must firstly provide "biocompatibility" which is the ability of the material to take place in tissues of the human body without any rejection or toxic effect. Biocompatibility assessment should include tests of acute systemic toxicity, cytotoxicity, hemolysis, intravenous toxicity, mutagenicity, oral toxicity, pyrogenicity and sensitization. In the case of non-biocompatibility (toxicity) characteristic of applied biomaterials (e.g. scaffolds and bone cements), implantation is concluded with irritation, inflammation and/or necrosis (death of cells in living tissue). [1,13-15,17-19].

3.1. Classification of Biomaterials

In most commonly, biomaterials are classified into four groups: polymeric biomaterials, metallic biomaterials, ceramic biomaterials and composite biomaterials. In order to mimic the bone structure, natural biopolymers (collagen/gelatin, chitosan, silk, alginate, peptides, etc.) and synthetic biopolymers (polyesters and copolymers) are used for tissue engineering applications. The well-known biometals are stainless steels (316 L), Ti and its alloys (Ti-6Al-4V) and Co–Cr alloys. Bioceramics are generally composed of alumina (Al_2O_3), zirconia (ZrO_2), titania (TiO_2), 45S5 Bioglass®, HA, TCP and corals. Also, polymer/ceramic, metal/ceramic and metal/polymer biocomposites have been investigated as bone graft substitutes.

Researchers also classified biomaterials in a different way. When biomaterials are placed in the body, some responses have been taken from the tissues depending on the structure of the material. The tissue-implant interaction mechanism varies depending on the response of the tissue and implant surface. Within this approach, biomaterials can be classified into 3 different groups: bioinert, bioresorbable and bioactive. The term of bioinert refers to the absence or minimal level of surrounded tissue response. Bioresorbable materials start to dissolve (resorbed) following the implantation and they replaced by tissue (bone) over a period of time. The bioactive characteristic, developed by Hench and his coworkers in 1969, leads the formation of a bone-like calcium phosphate layer at the tissue-implant interface upon immersion in biological fluids. Bone-like calcium phosphate layer has a close resemblance to the bone mineral in terms of composition and structure. That provides osteoconductivity and then chemically stable and strong implant-bone bond can be formed [12,20,21].

3.1.1. Bioceramics and bioactive ceramics

The different types of biomaterials present variable both advantages and disadvantages. Among them, biometals have superior mechanical properties due to their ductility and high fracture toughness whereas they possess high density and high concern about the biocompatibility. Because they can corrode *in vivo* environment and metallic elements cannot be tolerated in high contents by the body. The outcomes of corrosion are the disintegration of the implant (weakness) and harmful effects on the surrounding tissues and organs [15,16]. Biopolymers can be fabricated easily however, they are not strong as biometals, bioceramics and biocomposites [15]. In addition, biopolymers with

high molecular weight remain in the blood circulation for a long time. For instance, large ultra-high molecular weight polyethylene (UHMWPE) particles cannot be easily digested by cells, proteins and body fluids. Small particles have a negative effect on the body system like disrupting the integrity of cells, proteins and body fluids [16,22]. Although biocomposites give strength to structure and provide multiple properties depending on composition and structure, it is generally difficult to produce them. In addition, it is important that each constituent of the biocomposite must be biocompatible [15,16]. Even if bioceramics are brittle, they have significant advantages compared to biometals and biopolymers such as excellent biocompatibility, higher resistance to microbial attack, temperature, solvent conditions, pH changes, cyclic loads and packing under high pressure [21,23,24]. Due to these superior properties, bioceramics have been frequently preferred in recent years in orthopedic surgery and dentistry for repair and reconstruction. The worldwide market value of bioceramics was $431.4 million in 2005, dominating 50% of the market volume of biomaterials [12,25]. It is estimated that market value of bioceramics will reach $2.5 billion by the end of 2017 [26].

The first-generation bone graft substitutes were obtained from materials such as stainless steel, titanium and its alloys, alumina, zirconia, polymethylmethacrylate and ultra-high molecular weight polyethylene which have biocompatibility, bioinertness and also matchable physical properties with the bone tissue [1,20]. However, some biometals and biopolymers carry a risk of toxicity as mentioned before and all bioinert materials have high potential to be isolated from surrounding tissues through a fibrous capsule. Fibrous capsule with the thickness of several hundred micrometers forms in a few weeks up on implantation due to the foreign body reaction and micromovements took place at the tissue-implant interface. That leads to quick failure of implant (aseptic loosening) and then, a secondary surgery is needed for replacement [11,21]. To prevent both immune response and fibrous tissue formation, and to improve mechanical stability by bioactive fixation and osseointegration, second-generation bone graft substitutes were developed by Hench at the beginning of the 1970s. They are composed of bioactive ceramics such as HA, β-TCP, bioactive glass and apatite/wollastonite glass-ceramics which have excellent biocompatibility. Their surface chemistry provides mineralization through the heterogeneous nucleation and crystallization of bone-like apatite in terms of bioactivity. Subsequently, mineralization allows strong implant-bone bond and tissue ingrowth. Another type of second-generation bone graft substitutes is composed of bioresorbable

materials such as natural polymers (chitosan and hyaluronic acid), synthetic polymers (polylactide, poly(ε-caprolactone), polyglycolide), calcium carbonate ($CaCO_3$) and gypsum ($CaSO_4.2H_2O$). They can be resorbed by the body resulting of chemical breakdown under physiological conditions. The osteoconductivity and mechanical properties of bioresorbable materials can be improved by producing composites comprising bioactive ceramics. Nevertheless, adapting of degradation kinetics of bioresorbable materials is a challenge for the living tissue formation. The main requirement is to acquire matchable rate of degradation with the healing rate of the injured bone tissue. Furthermore, the mechanical properties decrease while resorption is proceeding. Therefore, bioactive ceramics have attracted much more attention due to their excellent biocompatibility, very high bioactivity and moderate mechanical properties with a lack of any fibrous tissue formation, immune response and non-matchable rate of degradation [1,11,16,20,27,28].

3.1.1.1. Bioactivity mechanism

The bioactivity characteristic of ceramics can be assessed *in vitro* by providing the formation of apatite layer on ceramic surfaces in simulated body fluids (SBFs). In 1991, Kokubo et al. had firstly prepared original SBF in order to predict bone activity *in vitro* which has closed ion concentrations to human blood plasma. Nowadays, the lactated Ringer's solution (LRS, also called as Lac-SBF: Lactated-Simulated Body Fluid) is widely used in hospitals due to no adverse effects reported in patients. Lac-SBF has ions in concentrations equal to that of human blood plasma and 22 mM Na-Lactate which is presented in the human body [29,30]. Ion concentrations of human blood plasma, original SBF and Lac-SBF are given in Table 3.1. [30,31].

Table 3.1. *Ion concentrations of human blood plasma, simulated body fluid (SBF) and lactated Ringer's solution (Lac-SBF)*

Ion Concentration [mM]	Na^+	K^+	Mg^{2+}	Ca^{2+}	Cl^-	HCO^-_3	HPO_4^{2-}	SO_4^{2-}	Na-Lactate
Human Blood Plasma	142.0	5.0	1.5	2.5	103.0	27.0	1.0	0.5	-
Original SBF	142.0	5.0	1.5	2.5	148.8	4.2	1.0	0	-
Lac-SBF	142.0	5.0	1.5	2.5	103.0	27.0	1.0	0.5	22

Researchers figured out the bone activity and bone formation mechanism *in vivo* following to *in vitro* assessments. In the lights of that, it is known that after implantation of bioactive materials (bioactive ceramics) into tissue (bone tissue), a bone-like calcium phosphate layer is mineralized at the tissue-implant interface *in vivo* through bioactivity mechanism which includes five steps at the following [11,32,33]:

- Exchange of alkali ions with hydrogen ions from body fluids leading to an increase in the interfacial pH
- Network dissolution by breaking the Si-O-Si bonds and then formation of silanol (SiOH) groups
- Polymerization of the SiO_2-rich layer with the condensation of silanol groups
- Formation of a $CaO\text{-}P_2O_5$ rich film resulting of the migration of Ca^{2+} and PO_4^{3-} groups onto the surface of silica-rich layer
- Crystallization of amorphous $CaO\text{-}P_2O_5$ rich film within hours by incorporation of hydroxyl (OH^-) and carbonate (CO_3^{2-}) anions

As stated above hydroxycarbonate apatite (HCA) layer is mineralized *in vivo* through bioactivity mechanism. The non-stoichiometric HCA is known as "dahllite" or "biological apatite". Besides the HCA and biological apatite, a number of calcium phosphate-based compounds have been detected along with HA in the hard and pathological tissues. These biologically relevant calcium orthophosphates have great potential to be used as bioactive ceramics for bone substitution. The Ca/P ratio, designation, abbreviation and chemical formula of biologically relevant calcium orthophosphates are given in Table 3.2.

Table 3.2. *The list of biologically relevant calcium orthophosphates*

Ca/P Ratio	Compound	Abbr.	Chemical Formula
0.5	Monocalcium phosphate monohydrate	MCPM	$Ca(H_2PO_4)_2.H_2O$
0.5	Monocalcium phosphate anhydrous	MCPA	$Ca(H_2PO_4)_2$
1.0	Dicalcium phosphate dihydrate, "Brushite"	DCPD	$CaHPO_4.2H_2O$
1.0	Dicalcium phosphate anhydrous, "Monetite"	DCPA	$CaHPO_4$
1.33	Octacalcium phosphate	OCP	$Ca_8(HPO_4)_2(PO_4)_4.5H_2O$

Table 3.2. (continued) *The list of biologically relevant calcium orthophosphates*

Ca/P Ratio	Compound	Abbr.	Chemical Formula
1.5	α-Tricalcium phosphate	α-TCP	$Ca_3(PO_4)_2$
1.5	β-Tricalcium phosphate	β-TCP	$Ca_3(PO_4)_2$
1.5-1.67	Calcium-deficient hydroxyapatite	CDHA	$Ca_{10-x}(HPO_4)_x(PO4)_{6-x}.(OH)_{2-x}$ (0<x<1)
1.67	Hydroxyapatite	HA	$Ca_{10}(PO_4)_6(OH)_2$
2.00	Tetracalcium phosphate, "Hilgenstockite"	TTCP	$Ca_4O(PO_4)_2$
1.2-2.2	Amorphous calcium phosphate	ACP	$Ca_x(PO_4)_y.nH_2O$

After the crystallization of bone-like calcium phosphate layer at the tissue-implant interface, the stages of the surface reaction play a crucial role on the growth of bone tissue which are [11,32,33]:

- Biochemical adsorption of growth factors on HCA layer
- Action of macrophages
- Attachment of stem cells
- Differentiation of stem cells to osteoblasts and proliferation of osteoblasts
- Generation of bone matrix
- Crystallization of bone matrix
- Growth of bone tissue

3.1.1.2. CaO-MgO-SiO_2 based bioactive ceramics

Bioactive ceramics have been widely used during last four decades as bone graft substitutes owing to their excellent biocompatibility and bioactivity where bone-like apatite layer leads to osteoconductivity and then the formation of chemically stable and strong implant-bone bond. Among bioactive ceramics, CaO-MgO-SiO_2 based bioactive ceramics have attracted growing interest due to their not only excellent biocompatibility and bioactivity, but also improved mechanical properties and superior biologic properties.

Monticellite ($CaMgSiO_4$), diopside ($CaMgSi_2O_6$), akermanite ($Ca_2MgSi_2O_7$), merwinite ($Ca_3MgSi_2O_8$) and bredigite [$Ca_7MgSi_4O_{16}$] are the members of CaO-MgO-SiO_2 system [10,28,34-39]. It is known that the chemical composition, stoichiometry and ionic substitution (ion types and concentration) of calcium phosphate-based bioceramics play a key role in their properties and determines biocompatibility, bioactivity,

biodegradability and fracture toughness [40]. Previous studies based on Ca, Mg and Si-containing bioactive ceramics show that Ca and Si ions could stimulate osteoblast proliferation, gene expression, bone mineralization and collagen synthesis [1]. Also, Mg ions affect the phenotype of osteogenic cells; directly stimulate osteoblast differentiation and proliferation; modulate the affinity of the osteoblasts to implants; considerably promote osteoblast adhesion by bonding to cell membrane adhesion receptors (integrins); and provide surface modification leaded bioactivity *in vitro* and *in vivo*. Furthermore, Mg improves mechanical properties of bioactive ceramics due to strong Mg-O bonds [1,28,34,39].

$CaO\text{-}MgO\text{-}SiO_2$ based bioactive ceramics can be accepted as third generation bone graft substitutes on the concept of bone tissue engineering because they not only present superior biological performance as mentioned before but also can enhance further the bone repair and regeneration by incorporating bone progenitor cells and growth factors [1]. Therefore, $CaO\text{-}MgO\text{-}SiO_2$ based bioactive ceramics hold great potential to take a place in the market. For instance, the usage of Ca and Mg-containing cement material (Osteocrete; Bone Solutions, Inc., Dallas, TX) has already approved by FDA (U.S. Food and Drug Administration) as a bone void filler for bone tissue regeneration.

4. MONTICELLITE BIOACTIVE CERAMICS

4.1. Structure, Properties and Application Areas of Monticellite Bioactive Ceramics

Among $CaO\text{-}MgO\text{-}SiO_2$ based bioactive ceramics, monticellite bioactive ceramics have received much more attention due to improved biologic, mechanical and thermal properties.

Monticellite belongs to the olivine group which includes a number of silicates crystallizing in an orthorhombic space group Pmnb. The structure of monticellite was firstly investigated by Brown and West in 1927. Onken stated the lattice parameters of monticellite obtained by X-Ray data as a:4.822 Å, b:11.108 Å, c:6.382 Å. Independent SiO_4 tetrahedra are linked by divalent atoms in six-fold coordination. There are two non-equivalent octahedral sites. Ca ions occupy the sites on the mirror planes and Mg ions are at the centers of symmetry. Each Ca and Mg is octahedrally coordinated by O atoms [41,42]. Crystal structure of monticellite drawn by Crystal Maker software is illustrated in Fig. 4.1.

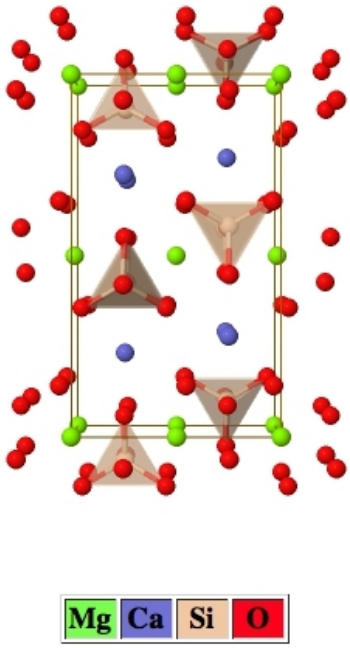

Figure 4.1. *Crystal structure of monticellite*

Among CaO-MgO-SiO_2 based bioactive ceramics, monticellite bioactive ceramics have the highest content of Mg. Hence, monticellite has the advantage to provide superior biologic properties (e.g. stimulating osteoblast differentiation and proliferation, promoting osteoblast adhesion, etc.) for the reasons explained before.

Table 4.1. *Mechanical properties of bone and bioactive ceramics*

Tissue / Material	Young's Modulus (GPa)	Fracture Toughness (MPa $m^{1/2}$)
Cortical Bone	7-30	2-12
Spongy Bone	0.5-0.05	-
HA	67-110	0.86-1.0
Bioglass® 45S5	35	0.7-1.1
Monticellite	45	1.65
Akermanite	56	1.53
Merwinite	49	1.57
Diopside	170	3.5
Bredigite	43	1.57

Young's modulus and fracture toughness values of cortical bone, spongy bone, HA, Bioglass® 45S5 and CaO-MgO-SiO_2 based bioactive ceramics are given in Table 4.1. Young's modulus and fracture toughness values of cortical bone and spongy bone which were obtained by longitudinal loading are given in a wide range because the mechanical properties of bone change depending on the anatomical locations; load directions; gender, age and health condition of patient; microstructure, porosity, length and mineralization of bone tissue [1,5,43]. A few studies report mechanical properties of CaO-MgO-SiO_2 based bioactive ceramics. Comparable results for monticellite, akermanite and merwinite ceramics, produced by the same route using identic starting materials, are obtained by only one research [34]. Related values for diopside and bredigite in Table 4 were adapted from different studies [39,44]. It is important to explain before making a comparison that all CaO-MgO-SiO_2 based bioactive ceramics given in Table 4.1. had been densified by researchers and they have closed relative densities in the range of 91 and 94 %.

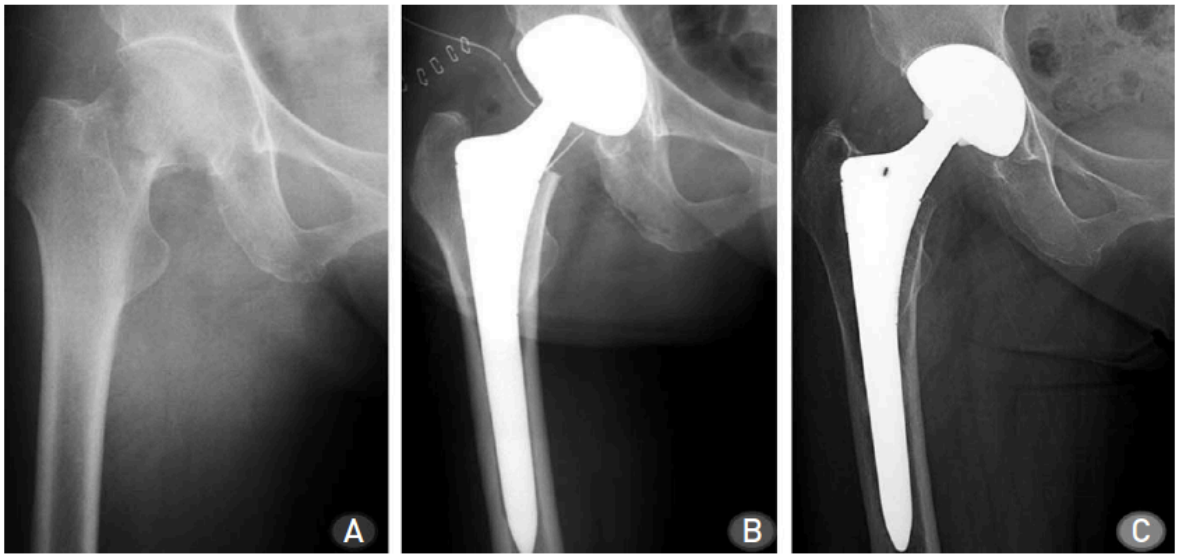

Figure 4.2. *Radiographs of right femur a) preoperative radiography, b) immediate postoperative radiography and c) postoperative radiography in 56th month after total hip arthroplasty*

Young's modulus and fracture toughness are the most critical mechanical properties of bioactive ceramics. Following to implantation, both bone and implant carry load instead of solely bone originally. When the bioactive ceramic as a bone graft substitute is stiffer (has higher Young's modulus) than the surrounded bone tissue, it takes over more stress than usual and bone is subjected to reduced stress. This phenomenon is called stress shielding. Stress shielding leads to a decrease in bone mass (bone resorption) and it results

in failure of implant. Therefore, it must be avoided from Young's modulus mismatch between bone and bioactive ceramic implant [25,45]. Kang et. al [46] conducted a clinical study in which thirty-seven hip joint replacements for thirty-one patients were evaluated over a minimum four-year period. VerSys Fiber Metal Taper Hip Prosthesis (FMT; Zimmer Inc., Warsaw) was implanted which has a circumferential titanium fiber-mesh surface located proximally, a midshaft circumferential corundum surface extending longer laterally and a polished, tapered distal part [47]. Fig. 4.2. shows the preoperative and postoperative radiographs of right femur in 62 years old woman. Neck fracture could be seen on the preoperative radiography in Fig. 4.2. (a). Immediate postoperative radiography in Fig. 4.2. (b) and postoperative radiography in Fig. 4.2. (c) indicates that hip replacement by uncemented implants caused stress shielding which is more obvious after 56 months. The clinical results show that thigh pain was noticed in 6 hips (16%) and proximal femoral bone resorption by stress shielding was observed in 32 hips (86.5%).

Another concern related to bioceramics is fracture toughness. If bioceramics are implanted into the loadbearing areas, fracture toughness gains more importance. Hence, fracture toughness should be as close as possible to that of cortical bone to avoid failure during long-term use [25,48]. In the light of this information, it is reported that well-known HA ceramics have inhibited its extensive applications to non-load-bearing areas due to poor mechanical properties and they carry a risk of bone atrophy occurred followed by stress shielding [28]. However, Bioglass® 45S5, bredigite and monticellite have closest Young's Modulus values to that of cortical bone. Furthermore, monticellite has highest fracture toughness among them with the value of 1.65 $MPa.m^{1/2}$. Therefore, monticellite ceramics have attracted more attention due to improved mechanical properties for the applications of bone void filling. They can be used in the forms of bulk pellets as a scaffold and powder as a bone cement.

Table 4.2. *Thermal expansion coefficients of $TiAl_6V_4$, HA and monticellite*

Material	**Thermal Expansion Coefficient ($^oC^{-1}x10^{-6}$)**
Ti-6Al-4V	10.03
HA	13.4
Monticellite	10.76

Another application area is the coating of bioactive ceramics on Ti-6Al-4V alloys. Nowadays, Ti-6Al-4V alloys are frequently used in reconstructive total hip surgeries and they are coated with HA to provide bone-implant integrity. Thermal expansion coefficients (CTEs) of $TiAl_6V_4$, HA and monticellite are given in Table 4.2. However, the coating of HA suffers from poor adhesion to the Ti-6Al-4V alloy substrate resulting from non-matchable thermal expansion coefficient [28,45]. Monticellite has closer CTE value to that of Ti-6Al-4V alloy compared to HA. That makes monticellite bioactive ceramics promising candidates for the application of coating on Ti-6Al-4V alloy.

4.2. Production Techniques of Monticellite Bioactive Ceramics

A careful survey of the literature shows that monticellite bioactive ceramics had been produced by the same method. Researchers in the same group prepared the starting materials by mixing tetraethyl orthosilicate ($(C_2H_5O)_4Si$, TEOS), magnesium nitrate hexahydrate ($Mg(NO_3)_2.6H_2O$) and calcium nitrate tetrahydrate ($Ca(NO_3)_2.4H_2O$) and then applied the sol-gel processes to synthesize monticellite powders [28,34]. In order to obtain monolithic monticellite ceramics, pellets were prepared by uniaxial pressing under 20 MPa using synthesized powders and prepared pellets were sintered at various temperatures (1350°C, 1400°C and 1480°C) for 6 hours. *In vitro* bioactivity tests and *in vivo* cytotoxicity tests showed that apatite crystals form and osteoblasts proliferate on the surface of monticellite ceramics as an evidence of bioactivity and biocompatibility characteristics, respectively.

As stated above, according to literature, monticellite bioactive ceramics were produced by the same methods including sol-gel synthesis and sintering. However, various starting materials and also, evaporation and drying processes were needed for sol-gel synthesis during conducted studies. In addition, sintering process was performed at high temperatures for long times. Therefore, it is clear that new methods are necessary to produce monticellite bioactive ceramics in a simple, cost-effective and eco-friendly way.

5. BORON DERIVATIVE WASTE

Turkey has almost 72% of the boron reserves in the worldwide with the total mass of 3.3 million tons. Boron deposits are located in specific regions which are Kırka/Eskişehir, Bigadiç/Balıkesir, Kestelek/Bursa and Emet/Kütahya [49]. Boron

minerals have a strategic importance due to their wide range of uses. For instance, borax pentahydrate ($Na_2O \cdot 2B_2O_3 \cdot 5H_2O$) has been used in many different sectors including ceramic, glass, agriculture, insulation, textile, detergent, construction, etc. since the 20th century [50]. Eti Mine Works General Directorate is the sole state-owned company authorized to control the boron deposits and refine the boron minerals. Almost all of the borax pentahydrate has been produced in Kırka Plant of Eti Mine Works in Eskişehir that the region is rich in tincal minerals. During the production of 1 million tons of borax pentahydrate ($Na_2O \cdot 2B_2O_3 \cdot 5H_2O$) from tincal ore, approximately 900.000 tons of solid boron derivative waste generated. The deposition of boron derivative waste in large quantities causes costly storage problems and serious environmental pollutions [50]. A permanent solution for these problems could not be found yet by the authorities. For this reason, different researches conducted lots of studies based on proper utilization strategies of boron derivative waste which is obtained from Eti Mine Kırka Plant. These studies are focused on the production of tiles, heavy clay ceramics and cement mortars incorporated by boron derivative waste or heat-treated boron derivative waste [51-56]. However, to the best of our knowledge, no study based on the production of monticellite bioactive ceramics using boron derivative waste obtained from Eti Mine Kırka Plant has been conducted. Therefore, the aim of the current study is synthesis and characterization of monticellite based bioactive ceramic powders obtained from boron derivative waste.

The aims of this study were the solid-state synthesis of monticellite based bioactive ceramic powders from boron derivative waste, the investigation of the effect of particle size on bone-like apatite formation ability of monticellite based ceramic powders and the determination of the cytotoxicity of monticellite based ceramic powder.

6. EXPERIMENTAL PROCEDURE

6.1. Characterization of Boron Derivative Waste

Boron derivative wastes provided from Eti Mine Works Kirka Borax Plant used as starting material. The chemical analysis of waste was determined by X-Ray Fluorescence (XRF) technique (Rigaku Primus ZSX) and the amount of boron oxide (B_2O_3) in waste was measured by titration method conducted at Ceramic Research Center (SAM, Anadolu University). The qualitative phase analysis of boron derivative waste was accomplished by X-Ray Diffractometer (XRD, Rigaku Rint 2200) with a scan speed of 0.5°/min in the 2θ range of 10-80°. Differential Thermal Analysis (DTA) and Thermogravimetry (TG)

were conducted by Netzsch STA 409 PC/PG under the atmospheric condition with the temperature range of 25-1100°C to provide information about changes in physical and chemical properties of waste as a function of increasing temperature. The particle size measurement of boron derivative waste was performed in distilled water media using a laser diffraction particle size analyzer (Mastersizer 2000, Malvern Instruments).

6.2. Synthesis of Monticellite Based Ceramic Powders

Monticellite ($CaMgSiO_4$) based ceramic powders (MBCPs) were prepared by solid state synthesis using boron derivative waste. The waste with a mass of 10 g charged onto a pure alumina plate. The heat treatments of wastes were carried out at 650°C and 800°C for various dwell times (1 min, 30 min, 1 h, 2 h, 3 h and 4 h) in an electrically heated furnace (KRC Lab. Eq.) under atmospheric pressure. After thermal processes, the refractory plate was taken out from the furnace quickly and quenched in air. The heating rate was kept 10°C/min. The reason of the quenching of synthesized powders to room temperature is to enhance apatite formation on powder surfaces through provided low crystallinity (weak network) and high dissolution rate. It is attributed that random loose network allows faster ions exchange during soaking in simulated body fluid (SBF) and enhance apatite formation ability indicating good bioactive response [57].

6.3. Characterization of Synthesized Powders

Following the solid-state synthesis, synthesized powders were crushed and ground to below 63 μm using a ring milling for 1min. mortar. The qualitative phase analysis of synthesized powders was accomplished using XRD with a scan speed of 0.5°/min in the 2θ range of 10-70°. The measurement time (2 hours) kept long in order to detect phases in low fraction. Microstructure analysis and semi-quantitative analysis of boron derivative waste and synthesized powders were performed using a scanning electron microscope (SEM, Supra 50VP, Zeiss) equipped with Secondary Electron (SE) and Energy-Dispersive X-ray Spectroscopy (EDS) detectors (Oxford Instruments).

6.4. Ball Milling of Monticellite Based Ceramic Powder

In order to decrease particle size of synthesized monticellite based ceramic powder at 800°C for 4 h (SP-800°C-4h), following to crushing of synthesized powder in agate mortar, particle size reduction of powder was performed using a planetary ball mill

(Pulverisette 6, Fritsch GmbH) at rotational speed of 400 rpm in ZrO_2 media (80 ml bowl volume and 10 mm ball diameter, Fritsch) under liquid free environment. 2.810 g of synthesized powder was charged for each ball-milling cycle. The weight ratio of ball-to-powder kept 10:1. Stearic acid ($CH_3(CH_2)_{16}COOH$, Merck KGaA) was used as deflocculant in 1 wt.% of charged powder. The milling times were set to 1, 2, 3 and 4 h. The direction of rotation of the planetary ball mill was reversed per hour and the sides of bowl were scraped down per hour. The stearic acid was evaporated by heat-treatment of ball-milled powders at 400°C for 2 h and then, the particle size measurement and qualitative phase analysis of crushed powder and ball-milled powders were performed by laser diffraction particle size analyzer and XRD under same conditions. The crushed synthesized powder in agate mortar and ball-milled synthesized powders for each milling time were called SP-800°C-4h-crushed, SP-800°C-4h-milled-1h, SP-800°C-4h-milled-2h, SP-800°C-4h-milled-3h and SP-800°C-4h-milled-4h, respectively.

6.5. Assessment of In Vitro Bioactivity

Prior to the assessment of *in vitro* bioactivity, crushed SP-800°C-4h and ball-milled SP-800°C-4h for 2 h were firstly compacted by uniaxial pressing. Secondly, the monticellite based ceramic powder wafers with dimensions of Ø13 x 3.5 mm^2 were subjected to cold isostatic press under 200 MPa. Finally, wafers were divided into two equal pieces to examine the thickness of formed bone-like apatite layer by SEM against the normalized cross-sectional area. For the assessment of *in vitro* bioactivity, wafers were soaked in Lac-SBF for 1, 2, 3, 5, 7, 14, 21 and 28 days at pH 7.40 and 36.5 ± 0.5°C. The ratio of wafer surface area to solution volume of Lac-SBF was kept 0.1 cm^2/ mL. The wafers were taken out after selected incubation times, rinsed with deionized water and dried for 24 h. The weight of wafers and pH of Lac-SBF were measured before and after the assessment. Also, the formation of bone-like apatite layer on the surfaces of monticellite based ceramic powder wafers were investigated by SEM equipped with SE and EDS detectors.

6.6. Assessment of In Vitro Cytotoxicity

6.6.1. Cell cultures and preparation of stock solutions

Three different cell lines were used for the experiments: nonmalignant murine fibroblast (3T3-L1, ATCC® CL-173™), human umbilical vein endothelium (HUVEC, ATCC® CRL-1730™), human normal skin fibroblast (CCD-1094Sk, ATCC® CRL 2120 ™). 3T3-L1 and HUVEC cell lines obtained from American Type Culture Collection (ATCC). CRL 2120 cell lines purchased from ATCC. CRL-2120 cells were cultured in Minimum Essential Medium Eagle (EMEM) supplemented with 10 % (v/v) fetal bovine serum, 1 % non-essential amino acid solution, penicillin (100 U/ mL)-streptomycin (100 µg/ mL) and sodium hydrogen carbonate. 3T3-L1 cells were maintained in Dulbecco's Modified Eagle's (DMEM) medium containing 10 % (v/v) fetal bovine serum, penicillin (100 U/ mL)-streptomycin (100 µg/ mL) and sodium hydrogen carbonate. HUVEC cells (HUVECs) were grown in Nutrient Mixture F12 HAM medium supplemented with 20 % fetal bovine serum, heparin (0.1 mg/ mL) and ECGS (0.5 mg/ mL). The cells were maintained at 37°C in a saturated humidified atmosphere containing 95 % air/ 5 % (v/v) CO_2. The monticellite based ceramic powder (MBCP) was sterilized at 180ºC for 3 h and freshly suspended at 1 mg/ mL concentration in cell culture medium without FBS and sonicated at room temperature for 15 min to avoid the aggregation/agglomeration of the particles before exposure. According to ISO 10993-12 standard [58], medical device materials can be delivered to a biological test system such as a cell culture in a measurable dose. Defining specific doses of the substances of interest is generally not possible. Generally speaking, the surface area ratio should be used whenever possible, with a mass-to-volume ratio used only for the testing of irregularly shaped devices or representative device components. Therefore, in the present study, the cell exposed final concentrations of 10, 50, 100, 200, 400, 500 and 800 µg/ mL in the cytotoxicity assays. Material concentrations are determined in a wide range by mass-to-volume ratio due to representative monticellite based ceramic powder composed of particles with irregular shapes.

6.6.2. Cell viability assays

The biocompatibility of a material is crucial in branding it as a biomaterial. Cell viability assays widely accepted that *in vitro* testing procedures are of considerable importance in cytotoxicity investigations of a biomaterial [59]. According to International

Standard (ISO 10993-5) methods [60], MTT and NRU assays can be used for this evaluation. As viability is determined by various cellular processes, different endpoints are currently to assess the actual state of cultured cells *in vitro*. Cytotoxic potential of MBCP was determined by MTT and NRU assays based on different cellular mechanisms depending on the damaged region.

6.6.3. Mitochondrial activity (MTT) assay

The cytotoxic effect of MBCP was determined by using *in vitro* colorimetric MTT assay [61]. Cells (5 x 10^3 cells/well) were seeded into 96-well microtiter tissue culture plates having a final volume of 100 µl. After 24 h of the attachment, the cells were treated with different concentrations (10, 100, 200, 400, 500 and 800 µg/ mL) of MBCP in the culture medium. Eight replicate wells per concentration were used and all experiments were repeated in triplicate. Solvent control (ultra-pure water) was assayed also in parallel. The cells were incubated for 24 and 48 hours with test material and MTT dye was added 4 h prior to completion of incubation periods. The medium from each well was discarded and resulting formazan crystals were solubilized by adding 100 µl of dimethylsulphoxide (DMSO) and quantified by measuring absorbance at 570 nm in an ELx808 Absorbance Microplate Reader (Bio-Tek, USA). All data expressed as means ± standard deviation (SD) using SPSS (Statistical Package for Social Sciences) software. The values were presented as a viability compared with control wells (the mean optical density of untreated cells was set 100 % viability), calculated One Way ANOVA (Analysis of Variance). All independent cytotoxicity experiments were repeated at least three times. In all cases, $p < 0.05$ was considered significant.

6.6.4. Neutral red uptake (NRU) assay

NRU cytotoxicity assay is widely used cell viability assay based on the ability of viable cells to incorporate and bind the supravital dye neutral red in the lysosomes. The assay was performed following the procedure as described by Borenfreund and Peurmer [62]. Briefly, CRL-2120, HUVEC and 3T3-L1 cells seeded into 96 well microtiter tissue culture plates and incubated for 24 h at 37ºC in a humidified atmosphere of 95 % air and 5 % CO_2 to allow cells to adhere to the culture plate. After the incubation period, cells were treated with monticellite based ceramic powder at the concentrations of 10, 100, 200, 400, 500 and 800 µg/ mL for 24 and 48 h. At the end of exposure time,

the test solution was removed and cells were carefully washed with phosphate buffer saline (PBS) and 100 µl of neutral red dye (50 µg/ mL) dissolved serum-free medium was added to each well. After 3 h incubation, the medium was discarded and cells were washed with a solution of 0.5 % formaldehyde and 1 % $CaCl_2$. Subsequently, 100 µl ethanol/acetic acid solution were added to all wells and cells were incubated 20 min to extract dye from the cells and to form a homogeneous solution. Absorbance was measured at 540 nm in ELx808 Absorbance Microplate Reader (Bio-Tek).

6.6.5. JC-1 staining assay

JC-1 (5,5'6,6' - tetrachloro - 1,1'3,3' - tetraethylbenzimidazol - carbocyanine iodide) staining assay was used to examine the effect of MBCP on the mitochondrial membrane potential of CRL 2120 cells [63]. Cells were grown on cover slips (Marienfeld) at a density of 25 x 10^4 cells per 12 well and treated for 24 hours with different concentrations (50, 100, 200, 400 and 800 µg/ mL) of the test material. Untreated medium controls and solvent controls (ultra-pure water at a final concentration of 0.1 %, v/v) were used also in parallel. Following media aspiration, cells were washed with PBS to clean the particle residues. JC-1 dye was prepared with 2 µM final concentration and added to each well. After 30 minutes incubation at 37ºC in a % 5 CO_2 incubator, dye removed and cells were washed with PBS. Coverslips were taken from the wells and examined with Olympus BX 50 fluorescence microscope at 570 nm. Images were captured with an Olympus DP71 camera using the DP Controller acquiring software (Olympus).

7. RESULTS AND DISCUSSION

7.1. Characterization of Boron Derivative Waste

Table 7.1. *Chemical composition (%, by weight) of boron derivative waste*

Oxides	SiO_2	CaO	MgO	B_2O_3	Na_2O	Al_2O_3	Fe_2O_3	SrO
Waste	18.9267	18.4677	13.5513	7.50	5.2884	2.3140	0.9111	0.7718
Oxides	SO_3	K_2O	BaO	Cs_2O	TiO_2	Cr_2O_3	P_2O_5	CuO
Waste	0.7656	0.7141	0.6627	0.1968	0.0763	0.0383	0.0246	0.0116

Loss on Ignition (1000°C): 29.7780

The chemical composition of boron derivative waste is given in Table 7.1. The loss on ignition (L.O.I) value below 1000°C was approximately 30 wt. %. According to

ASTM standard specification for glass and glass ceramic biomaterials for implantation (ASTM-F1538-03) the total content of heavy metal elements such as arsenic (As), cadmium (Cd), mercury (Hg), lead (Pb) should be maximum 50 ppm in bioceramics due to their toxic effects. The abundance of these heavy metal elements could be accurately detected at ppm level by XRF technique. XRF analysis results exhibit that there is no heavy metal elements existed in boron derivative waste.

It is reported that major elements in the waste including silicon, calcium, magnesium, boron and sodium considered essential and/or beneficial for bone metabolism. They stimulate collagen synthesis, enhance bone matrix mineralization and formation of apatite-like surface layers, improve mechanical properties of bone and prevent bone-related diseases. Morever, deprivation of them leads to adverse effects. Although some trace elements in the waste may have controversial or deleterious effects on human health [64], Ferreira and Goel [65] prepared bioactive glass compositions consist of mainly CaO, MgO, P_2O_5, SiO_2, CaF_2 compounds comprising as a doping agent at least one of the following elements: Na, K, Li, Ru, Cs, Fr, Sr, Bi, Zn, Ag, B, Cu, Mn, Fe and Ti or an oxide in a molar percentage between 0 - 10. It is stated that sintered powders derived from bioglass were able to promote the formation of carbonated hydroxyapatite layer upon immersion in SBF and powders could be used as bone substitutes and coatings for implants. In addition, Jung and Day [66], provided bioglass compositions for tissue repair or regeneration in mammals consisting of one or more director element compounds in a concentration of 0.05 to 5 wt. % comprising of Cu, Sr, Zn, Fe, Mn, Cr, V, Nb, Mo, W, Ba, Co, S, Al, Ti, Y, Mg, Si and/or Ni. The biocompatible characteristics of scaffolds were noticed after implantations *in vivo*. Considering these results obtained by different patent applications, boron derivative waste has still potential to use as a raw material for bio-based industrial production, however, the role of trace elements in toxicity needs to be elucidated.

Table 7.2. *List of abbreviations of compounds in boron derivative waste, their chemical formulas and their JCPDS card numbers for identification*

Abbreviation	Compound	Chemical Formula	JCPDS Card Number
DO	Dolomite	$CaMg(CO_3)_2$	36-0426
CA	Calcite	$CaCO_3$	05-0586
Q	Quartz	SiO_2	87-2096
TI	Borax Pentahydrate	$Na_2B_4O_7$-$5H_2O$	07-0277
K1	Kaolinite	$Al_2Si_2O_5(OH)_4$	29-1488

List of abbreviations of compounds in boron derivative waste, their chemical formulas and their JCPDS card numbers are given in Table 7.2. Fig. 7.1. illustrates the XRD pattern of boron derivative waste. Dolomite ($CaMg(CO_3)_2$, ICDD 36-0426), calcite ($CaCO_3$, ICDD 05-0586), quartz (SiO_2, ICDD 87-2096), borax pentahydrate (tincalconite, $Na_2B_4O_7$-$5H_2O$, ICDD 07-0277) and kaolinite ($Al_2Si_2O_5(OH)_4$, ICDD 29-1488) were detected as crystalline phases, confirming the XRF results. Two highest peaks in intensity represent dolomite and calcite crystalline phases.

DTA and TG/DTG curves of boron derivative waste are illustrated in Fig. 7.2. On DTA curve, four characteristic endothermic peaks were identified at 151.7ºC, 639.9ºC, 775.8ºC and 1080.7ºC. Three exothermic peaks were observed at 341.5ºC, 704.5ºC and 910.3ºC. In addition, all endothermic events are accompanied by the mass loss as shown on the TG/DTG curves. The highest mass loss (18.76%) was observed in the temperature range of 500ºC - 700ºC and the total mass loss was 32.28%. Almost no more mass change was occurred above 800ºC.

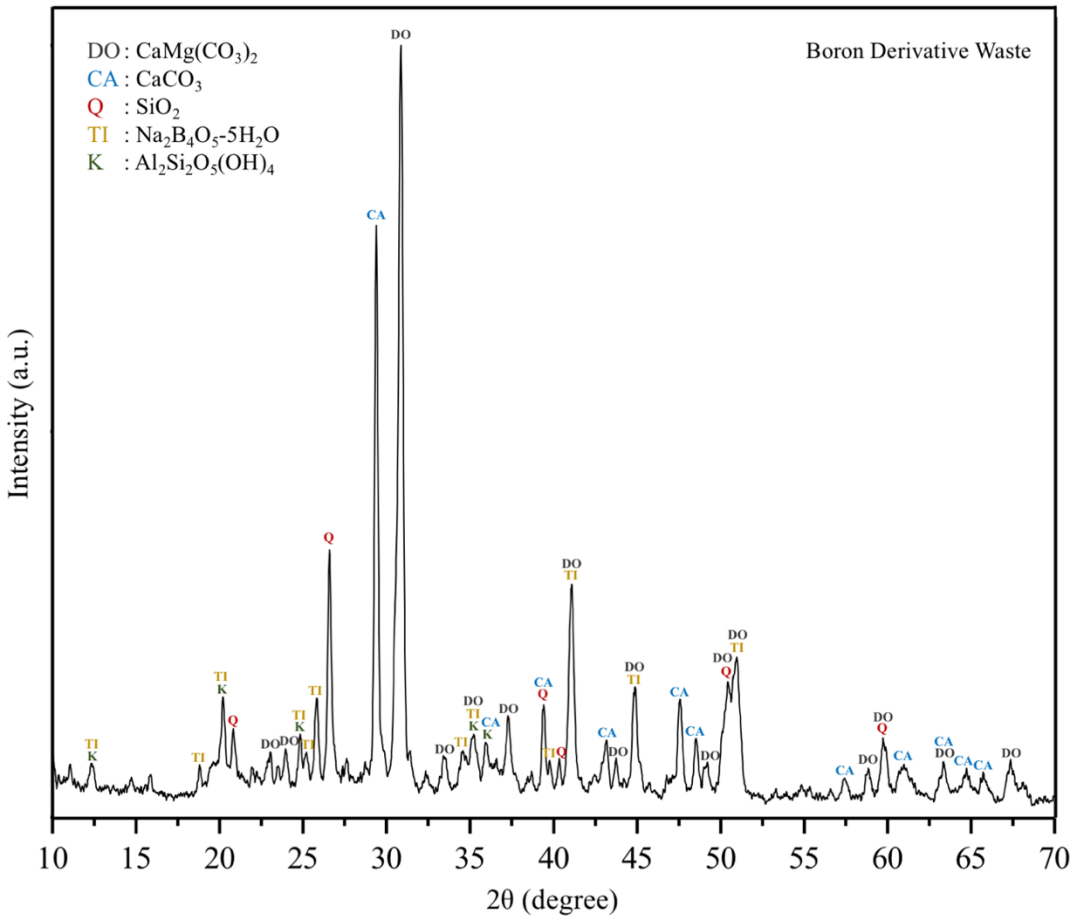

Figure 7.1. *XRD pattern of boron derivative waste*

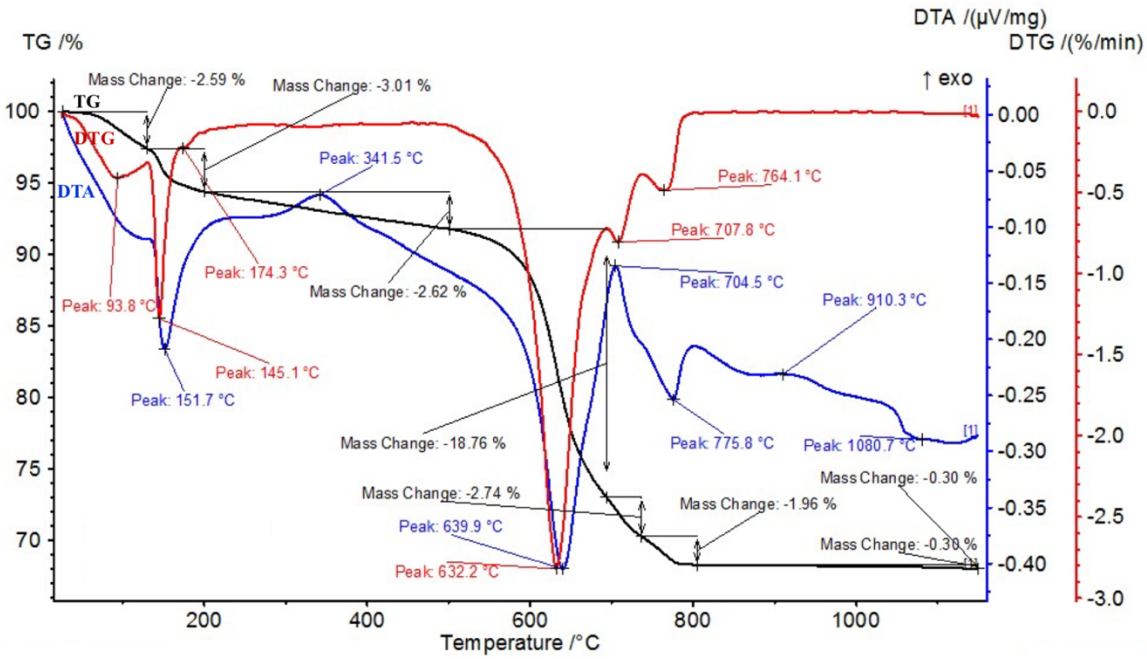

Figure 7.2. *DTA and TG/DTG curves for boron derivative waste*

Three characteristic particle diameters (d) for boron derivative waste determined by laser diffraction particle size analysis. The obtained results show that d10 value is 0.414 μm, d50 value is 0.823 μm and d90 value is 2.776 μm for boron derivative waste. The waste consists of fine particles with narrow particle size range. The reason of that is associated with the refinement processes of boron minerals which are occurred in Eti Mine Kırka Plant prior to the supplying of boron derivative waste.

7.2. Thermodynamic Approach

The Gibbs free energy (Gibbs function) is a thermodynamic function based on enthalpy and entropy of the system. It is highly significant to investigate reactions at constant temperature or pressure. It provides the main basis for the criterion of spontaneity of chemical process and chemical equilibrium. The change of Gibbs free energy (ΔG) at constant temperature: $\Delta G = \Delta H - T\Delta S$, where H denotes enthalpy, S entropy and T temperature.

According to the second law of thermodynamics, the total entropy increases in the spontaneous process, in this way the Gibbs free energy of the system decreases. Therefore, a chemical reaction at specified temperature and pressure proceeds in the direction of decreasing Gibbs free energy. When the Gibbs free energy reaches a minimum value, the chemical reaction stops and chemical equilibrium is established [67,68].

As stated before, the aim of present study is solid state synthesis of monticellite based ceramic powders from boron derivative waste and this waste is rich in dolomite and calcite. Thus, the thermal decomposition of both dolomite and calcite must be provided first in order to synthesize powders. At this point, it is crucial to optimize the heat treatment temperature to proceed chemical reactions (7.1 and 7.2) for dolomite and calcite calcination under atmospheric pressure.

$$CaMg(CO_3)_2 \text{ (dolomite)} \Leftrightarrow CaO + MgO \text{ (periclase)} + 2\ CO_2(g) \quad (7.1)$$

$$CaCO_3 \text{ (calcite)} \Leftrightarrow CaO + CO_2(g) \quad (7.2)$$

In terms of calcination of calcite and dolomite-rich clay materials, it is stated that dolomite and calcite started to decompose at 600ºC and 800ºC by decarbonization [69]. Furthermore, Sasaki et al. explained that calcination of dolomite and calcite in natural

dolomite commenced around 600ºC and above 700ºC [70]. For this reason, two endothermic peaks at 639.9ºC and 775.8ºC and also high mass loss were related to the thermal decomposition of dolomite and calcite. Even if the starting temperatures of dolomite and calcite calcination were expressed as 600ºC and in the range of 700ºC-800ºC in literature and also two endothermic peaks at 639.9ºC and 775.8ºC on DTA and TG/DTG curves indicate the thermal decomposition temperature of dolomite and calcite, to obtain thermodynamic data by using a thermochemical software certainly aids to specify more accurate heat treatment temperatures.

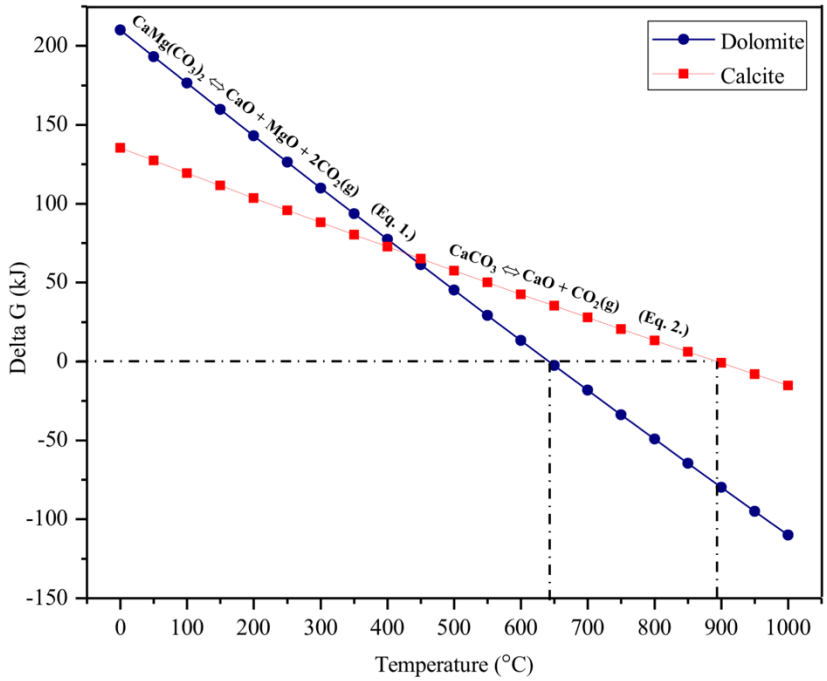

Figure 7.3. *Delta G-Temperature diagram for chemical reactions of dolomite and calcite calcination (7.1 and 7.2)*

Fig. 7.3. which was drawn by using FactSage Thermochemical Software, demonstrates Delta G-Temperature diagram for dolomite and calcite calcination reactions (7.1 and 7.2) under constant atmospheric pressure (1.01325 bar). Delta G values are negative above 645ºC for dolomite calcination reaction and 895ºC for calcite calcination reaction. It means that dolomite calcination reaction above 645ºC and both dolomite and calcite calcination reactions above 895ºC can proceed spontaneously in theoretically. Therefore, heat treatment temperatures were selected as 900ºC and 650ºC considering both Delta G-Temperature diagram and DTA & TG/DTG curves. It is thought that

selected temperatures give reactants adequate energy to overcome an activation energy barrier of height Ea in order to achieve the activated complex state and proceed to products in terms of phase formation, transformation and decomposition [71].

7.3. Characterization of Monticellite Based Ceramic Powders

7.3.1. Phase evolution of synthesized powders

XRD is a frequently used technique in worldwide for the qualitative phase analysis of materials. Through phase analysis obtained XRD patterns not only allow to basic search/match process but also give some information on the structure: (i) the angular position of diffraction lines give the size and shape of the unit cell, (ii) the intensity of the diffraction lines depends on the type of atoms and the crystallographic orientation, and (iii) their shape are used to get information on instrumental broadening, particle size and deformation [72].

Table 7.3. *List of abbreviations of compounds used in this work, their chemical formulas and their JCPDS card numbers for identification*

Abbreviation	Compound	Chemical Formula	JCPDS Card Number
DO	Dolomite	$CaMg(CO_3)_2$	36-0426
CA	Calcite	$CaCO_3$	05-0586
Q	Quartz	SiO_2	87-2096
TI	Borax Pentahydrate	$Na_2B_4O_7$-$5H_2O$	07-0277
K	Kaolinite	$Al_2Si_2O_5(OH)_4$	29-1488
D1	Diopside	$CaMgSi_2O_6$	78-1390
D2	Calcium Magnesium Silicate	$Ca_{0.8}Mg_{1.2}Si_{1.99}O_6$	72-1499
M	Monticellite	$CaMgSiO_4$	76-0727
A	Akermanite	$Ca_2MgSi_2O_7$	83-1815
F	Forsterite	Mg_2SiO_4	76-0563
Z	Zeolite LTA	$Na_6(AlSiO_4)_6$	42-0217
TA	Calcium Borate	$Ca_3B_2O_6$	26-0347
C1	Calcium Magnesium Borate	$CaMgB_2O_5$	73-0618

In the light of that information, phase analysis of monticellite based ceramic powders was accomplished by XRD technique. List of abbreviations of compounds (phases) used in this work, their chemical formulas and their JCPDS card numbers are

given in Table 7.3. Fig. 7.4. shows a schematic representation of mineralogical transformations (formation/ decomposition of phases) in boron derivative waste during heat treatments at 650°C, 800°C and 900°C in the time interval (1 min - 4 h) according to XRD patterns.

In this research, considering XRD patterns of all synthesized powders, it is easily noticeable that chemical composition of each powder possesses phases in large quantities and that creates complex XRD patterns with a great number of major and minor peaks. Moreover, peaks of different phases interfere and overlap with each other. Therefore, search/match analysis was carried out in required periods of a long time indicating necessary precision. Also, it is important to state that in case of peaks of different phases overlap each other, abbreviation of a phase which has higher peak intensity is located upper-side in terms of indexing.

Sample Code / Phase & Formula		Waste	650°C 1min	650°C 30min	650°C 1hr	650°C 2hr	650°C 3hr	650°C 4hr	800°C 1min	800°C 30min	800°C 1hr	800°C 2hr	800°C 3hr	800°C 4hr	900°C 1min
Dolomite	$CaMg(CO_3)_2$														
Calcite	$CaCO_3$														
Quartz	SiO_2														
B. Pentahydrate	$Na_2B_4O_5$-$5H_2O$														
Kaolinite	$Al_2Si_2O_5(OH)_4$														
Diopside	$CaMgSi_2O_6$														
C. M. Silicate	$Ca_{0.8}Mg_{1.2}Si_{1.99}O_6$														
Monticellite	$CaMgSiO_4$														
Akermanite	$Ca_2MgSi_2O_7$														
Forsterite	Mg_2SiO_4														
Zeolite LTA	$Na_6(AlSiO_4)_6$														
Calcium Borate	$Ca_3B_2O_6$														
C. M. Borate	$CaMgB_2O_5$														

Figure 7.4. *Diagram representing phase transformations in boron derivative waste induced by heating at 650°C, 800°C and 900°C for dwell time range of 1 min - 4 h according to XRD patterns. Dark/ light bars indicate approximately abundance of phases*

7.3.1.1. Solid state synthesis at 650°C

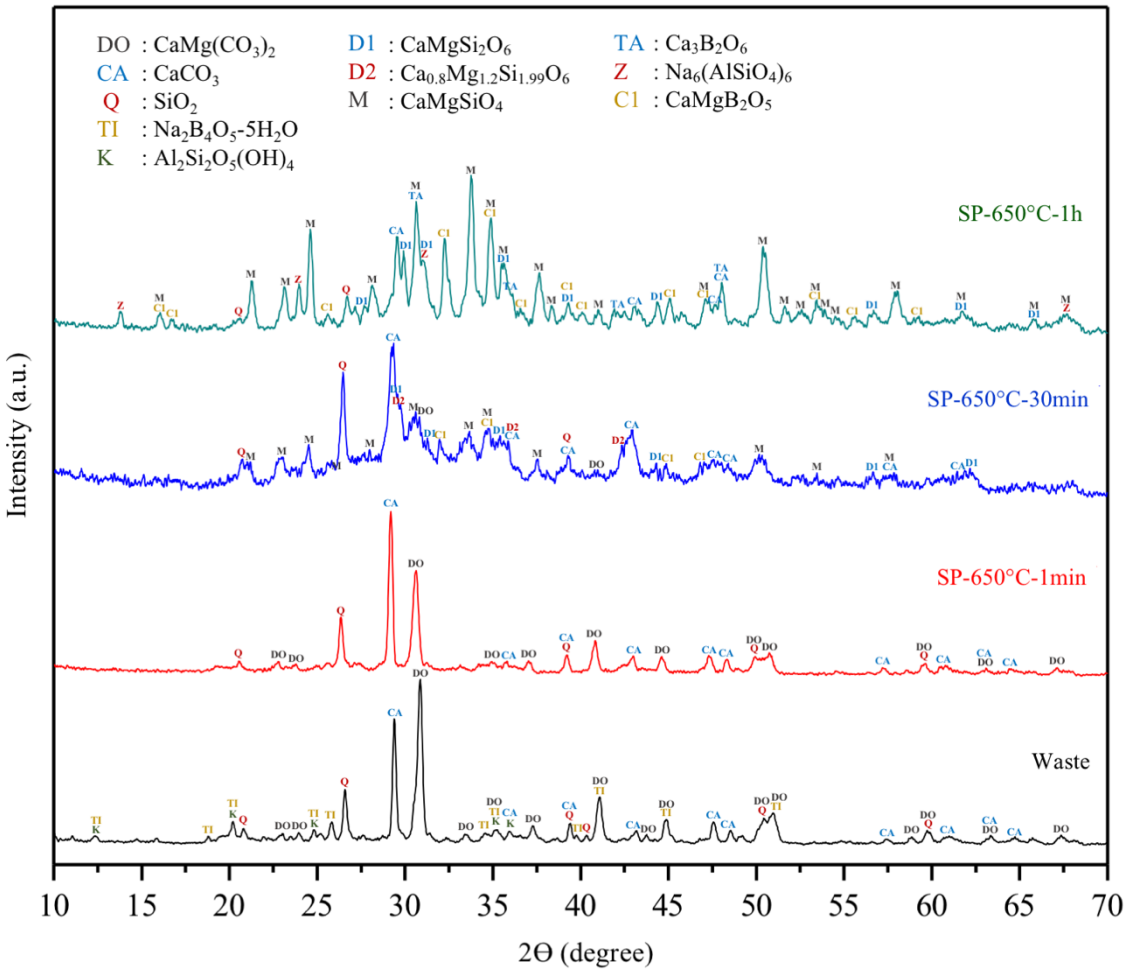

Figure 7.5. *XRD patterns of synthesized powders at 650°C for 1min, 30min and 1h compared to waste*

XRD patterns of synthesized powders at 650°C for 1 min, 30 min and 1 h compared to waste are shown in Fig. 7.5. According to Fig. 7.5., both boron derivative waste and SP-650°C-1min specimens contain the crystalline phases of calcite, dolomite and quartz. A decrease in peak intensities of dolomite was observed relatively because thermal decomposition of dolomite has already started at 650°C in 1 min. Borax pentahydrate and kaolinite phases no more existed. It is reported that the dehydration of borax pentahydrate ($Na_2B_4O_7$-$5H_2O$) occurred in two steps in a temperature range of 73ºC - 535ºC with the total weight loss of roughly 30% [73]. Firstly, 2.75 moles of crystal water were eliminated and crystal structure became amorphous. Secondly, the remainder 2 moles of water exist as hydroxyl groups and can be considered for molecular water. However, swelling of particles during removal of molecular water leads to the higher surface area and voids in

larger quantities. Furthermore, molecular water could only be removed by molecular decomposition which results in the formation of 1 mole Na_2O and 2 moles B_2O_3 compounds [73,74]. Thus, on DTA and TG/DTG curves, endothermic peak at 151.7ºC and mass loss of nearly 8% from room temperature to around 500ºC are associated with the removal of water within borax pentahydrate and also one exothermic peak at 341.5ºC is correlated with rehydration of borax pentahydrate during removal of molecular water. It is known that kaolinite ($Al_2Si_2O_5(OH)_4$) decomposes to amorphous metakaolinite ($Al_2Si_2O_7$) between 500ºC and 600ºC by removal of hydroxyl groups of silicate lattice [69,75,76]. These deductions explain why borax pentahydrate and kaolinite could not be detected by XRD with the increasing of heat treatment temperature to 650°C.

The studies focused on the calcination kinetics of dolomite and calcite expressed that, in the first step of decarbonisation, magnesium oxide and calcite formed along with releasing of 1 mole CO_2 gas in the temperature range of 600°C and 700°C. Then, the formation of CaO commenced simultaneously by decarbonisation of calcite between 700°C and 900°C [70,77]. For this reason, an increase in calcite content at 650°C after 1 min was expected due to high amount of calcite produced by dolomite calcination however, it is difficult to determine exactly increased calcite concentration without Rietveld Quantitative Phase Analysis. The multiphase quantitative analysis is based on the diffraction pattern intensity of a particular phase in a mixture of phases which depends on the concentration of that phase in the mixture. The relation between intensity and concentration is not generally linear [78]. Thus, the peak intensities related to phase concentrations were specified “relatively”.

For SP-650°C-30min specimen, calcite, dolomite, quartz, calcium magnesium silicate ($Ca_{0.8}Mg_{1.2}Si_{1.99}O_6$, ICDD 72-1499), diopside ($CaMgSi_2O_6$, ICDD 78-1390), monticellite ($CaMgSiO_4$, ICDD 76-0727) and calcium magnesium borate (kurchatovite, $CaMgB_2O_5$, ICDD 73-0618) were detected as crystalline phases. A sharp reduction in peak intensities of dolomite and an enhancement in amorphous content were noticed because of the decomposition of dolomite and the formation of new crystalline phases. The yielding of diopside and monticellite as metastable phases at dolomite–quartz and/or dolomite-calcite-quartz interfaces was attributed to theoretical chemical reactions of calcination products (MgO and CaO) with quartz in proper molar ratios (7.3 and 7.4). In 30 min dwell time at 650°C, the nucleation and growth of some non-stoichiometric crystals led to form calcium magnesium silicate phase as non-stoichiometric diopside.

The formation of calcium magnesium borate was ascribed to the reaction of B_2O_3 in liquid form as a decomposition product of borax pentahydrate with CaO and MgO as calcination products (7.5).

$$2SiO_2 + CaO + MgO \Leftrightarrow CaMgSi_2O_6 \text{ (diopside)} \quad (7.3)$$

$$SiO_2 + CaO + MgO \Leftrightarrow CaMgSiO_4 \text{ (monticellite)} \quad (7.4)$$

$$CaO + MgO + B_2O_3 \Leftrightarrow CaMgB_2O_5 \text{ (calcium magnesium borate)} \quad (7.5)$$

In the comparison of SP-650°C-1h with SP-650°C-30min, the dolomite was completely calcined and while peak intensities of calcite and quartz decreased, that of monticellite, diopside and calcium magnesium borate increased, relatively. That supports the phase formation mechanisms of diopside and monticellite which are stated above. Non-stoichiometric diopside (calcium magnesium silicate, $Ca_{0.8}Mg_{1.2}Si_{1.99}O_6$) transformed to stoichiometric diopside after 30 min. Moreover, zeolite LTA (dehydrated sodalite, $Na_6(AlSiO_4)_6$, ICDD 42-0217) and calcium borate (takedaite, $Ca_3B_2O_6$, ICDD 26-0347) were detected as minor crystalline phases. Low silica zeolites (LTA, framework type code of zeolites is given according to the classification of the International Zeolite Association) are represented by a general formula: 2 $Na_6(AlSiO_4)_6$ [79]. Rios Reyes et al. and Gualtieri et al. have synthesized pure zeolite LTA by alkaline fusion (thermal activation) at 600°C for 1 hour and hydrothermal synthesis using NaOH (powder and solution) and metakaolinite which was obtained from kaolinite-rich clay [80,81]. In accordance with this information, zeolite phase (LTA, $Na_6(AlSiO_4)_6$) was able to be obtained by the reaction of amorphous metakaolinite ($Al_2Si_2O_7$) with Na_2O which take place by dehydration of kaolinite and molecular decomposition of borax pentahydrate. In addition, the increasing of dwell time to 1 hour at 650°C led to the formation of CaO products in the higher content owing to higher amount of reactive calcite compounds. Hence, after formation of monticellite, diopside and calcium magnesium borate phases, excess CaO compounds was able to react immediately with B_2O_3 compounds to generate calcium borate, which is stable around 700°C according to $CaO\text{-}Al_2O_3\text{-}B_2O_3$ ternary phase diagram [82]. No free B_2O_3 groups were observed in XRD patterns due to its quite low melting point (450°C).

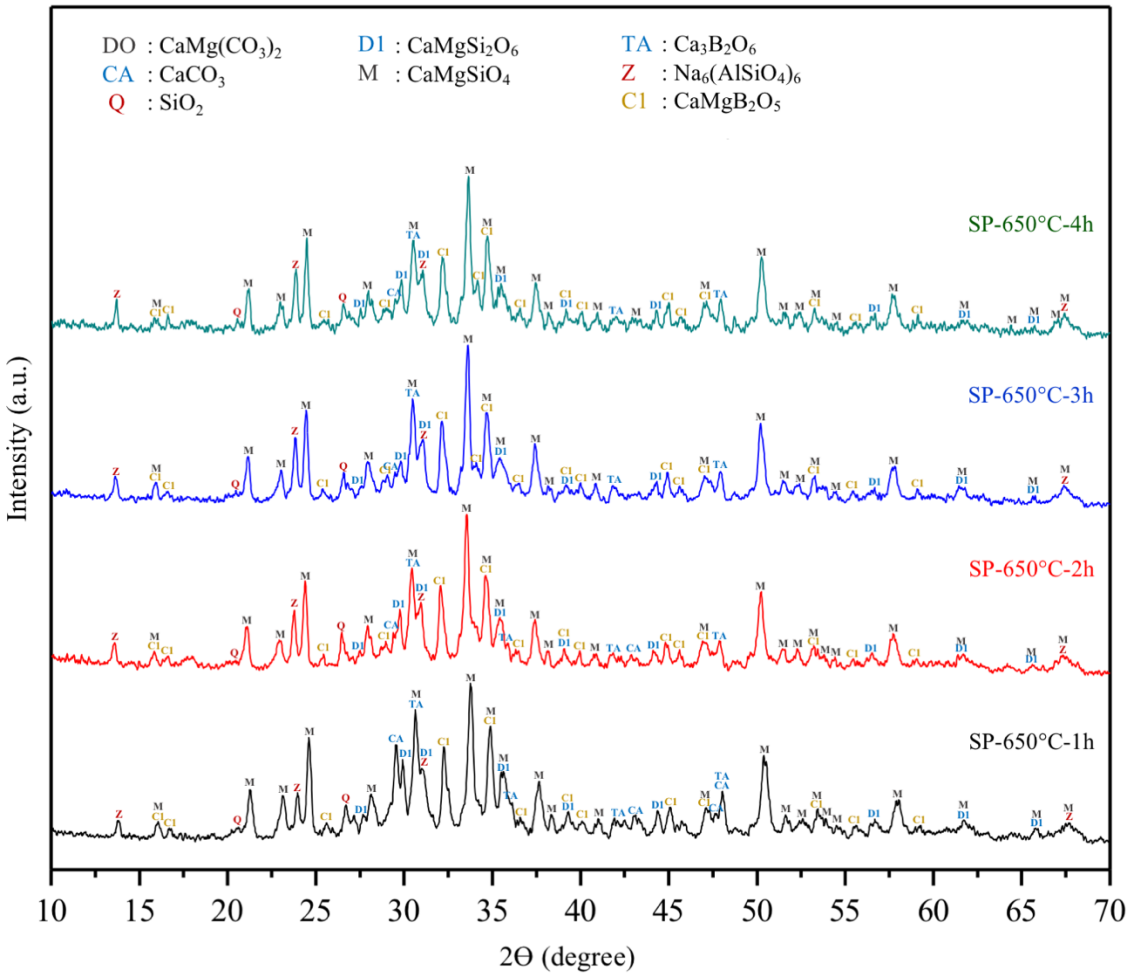

Figure 7.6. *Comparative XRD patterns of synthesized powders at 650°C for 1h, 2h, 3 h and 4 h*

Fig. 7.6. exhibits quite similar XRD patterns of SP-650°C-1h, SP-650°C-2h, SP-650°C-3h and SP-650°C-4h specimens. The existence of all phases was stable. The peak intensities of calcite significantly diminished for SP-650°C-2h, relatively. When dwell time gradually raised from 2 to 4 hours at 650°C, calcite peak in highest intensity became smaller.

Semi-quantitative information about crystallite size of a polycrystalline structure could be yielded by XRD technique. If the size of individual crystals is in the nanometer range, average crystallite size (L) can be calculated with well-known Scherrer Equation: $L=K.\lambda/\beta.\cos\theta$, where λ is the X-ray wavelength in nm, β is the peak width of the diffraction line at half maximum intensity in radian (FWHM) and K is a constant related to crystallite shape, generally taken as 0.9 [78,83]. According to Scherrer Equation, average crystallite size is inversely proportional to FWHM. XRD patterns of both liquids and amorphous solids characterized by an almost complete lack of periodicity, show a

broad halo instead of high sharp maxima at certain angles [78]. It is thought that monticellite and diopside were formed at 650°C just before 30th minute because FWHM is so high which indicates the quite low crystallite sizes just reached after the nucleation and crystal growth. A gradual decrease in amorphous condition and increase in crystallite sizes of calcium magnesium borate, diopside and monticellite were observed at 650°C from 30 minutes to 4 hours.

7.3.1.2. Solid state synthesis at 900°C

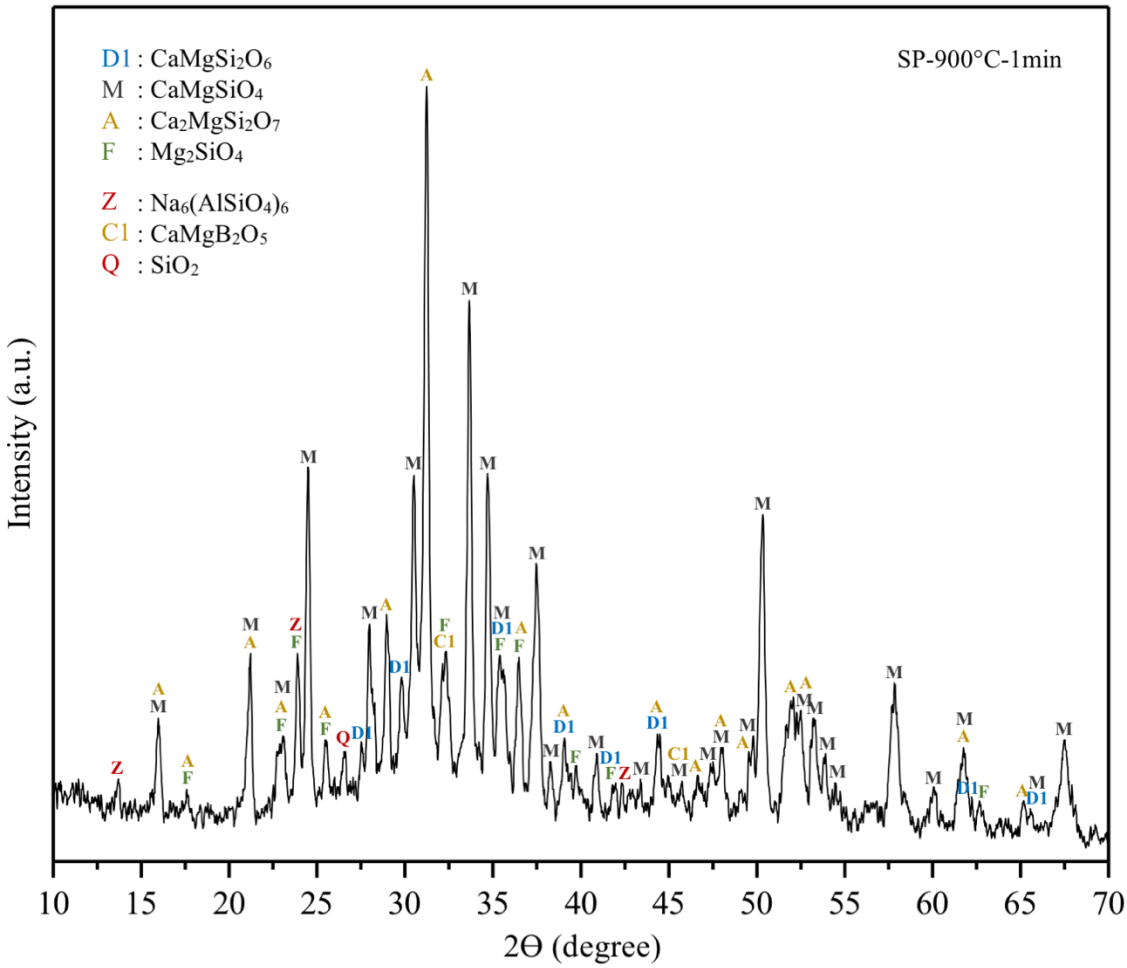

Figure 7.7. *XRD pattern of synthesized powder at 900°C for 1min*

The XRD pattern of heat-treated boron derivative waste at 900°C for 1 min is illustrated in Fig. 7.7. As shown in Fig. 7.7., the detected crystalline phases were monticellite, diopside, calcium magnesium borate, zeolite, quartz, akermanite ($Ca_2MgSi_2O_7$, ICDD 83-1815) and forsterite (Mg_2SiO_4, ICDD 76-0563) for

SP-900°C-1min specimen. Akermanite and forsterite was firstly detected with heat treatment at 900°C for 1min. High crystallinity for akermanite and monticellite, and a few amorphous contents resulting of newly formed and non-entirely crystallized forsterite phase were observed. Although calcination reaction of calcite is thermodynamically favored at 900°C under atmospheric pressure, dolomite and calcite was completely calcined until reaching 900°C. Almost zero mass change above 800ºC in TG/DTG curves confirms that calcite in boron derivative waste was thermally decomposed up to 800ºC. In accordance with this information, in order to investigate calcination behavior of calcite and phase formation mechanisms of Ca-Mg-Si based phases, it is decided to decrease heat treatment temperature to 800°C which is consistent with the literature [69].

7.3.1.3. Solid state synthesis at 800°C

XRD patterns of synthesized powders at 800°C for 1 min, 30 min and 1 h compared to waste are shown in Fig. 7.8. SP-800°C-1min specimen includes monticellite, diopside, akermanite, calcium magnesium borate, quartz, zeolite and calcite phases. While 1 hour dwell time was needed to complete calcination of dolomite at 650°C, the increment of temperature to 800°C assured thermal decomposition without long holding time. Unlike SP-900°C-1min, SP-800°C-1min sample does not comprise forsterite and calcite. Akermanite phase formation is correlated with theoretical chemical reaction (7.6) where the system is richer in CaO compared to diopside and monticellite formation reactions (7.3 and 7.4). In the comparison of SP-800°C-30min with SP-800°C-1min, the peak intensities of akermanite increased, that of diopside, calcium magnesium borate and zeolite relatively decreased and calcite disappeared. In other words, calcite phase was completely consumed according to XRD analysis. However, it is important to emphasize that detection limit (threshold) of XRD technique is minimum 1-2 vol.% [84]. For this reason, it can be stated that the required activation energy to complete calcite calcination, according to XRD patterns, was provided throughout the heat treatment of waste at 800°C for 30 min. With the increment of dwell time to 1 hour, a slight reduction in peak intensities of diopside and calcium magnesium borate progressed further. Moreover, a decrease in peak intensities of quartz was observed.

$$2SiO_2 + 2CaO + MgO \Leftrightarrow Ca_2MgSi_2O_7 \text{ (akermanite)} \quad (7.6)$$

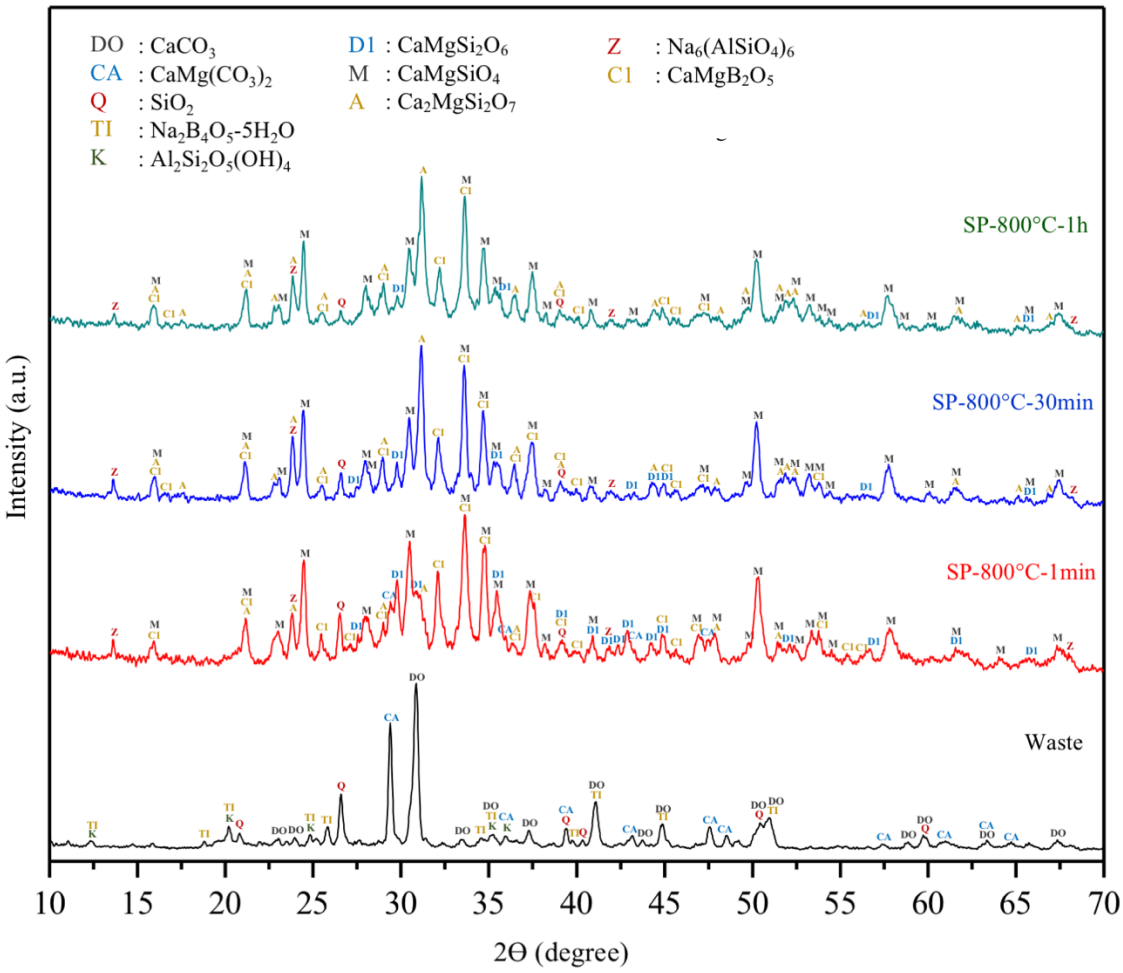

Figure 7.8. *XRD patterns of synthesized powders at 800°C for 1min, 30min and 1h compared to waste*

Comparative XRD patterns of synthesized powders at 800°C for 1 h, 2 h, 3 h and 4 h are given in Fig. 7.9. Both synthesized powders at 800°C for 1 hour and 2 hours contains same crystalline phases such as akermanite, monticellite, diopside, calcium magnesium borate, zeolite and quartz. Within the third hours, the fully consuming of quartz was identified. XRD patterns of synthesized powders at 800°C for 1, 2, 3 and 4 hours are similar and the existence of all crystalline phases in SP-800°C-2h except quartz remained up to 4 hours. SP-800°C-4h sample comprises monticellite, akermanite and calcium magnesium borate as major phases whereas diopside and zeolite exist as minor phases.

According to DTA and TG/DTG curves and obtained results, two other endothermic peaks at 639.9ºC and 775.8ºC with the highest mass loss (18.76%) in the temperature range of 500ºC - 700ºC are associated with calcination of dolomite and calcite. Two exothermic peaks are identified with crystallization of diopside &

monticellite at 704.5ºC and akermanite at 910.3ºC. Also, the softening of boron derivative waste is united with last endothermic peak at 1080.7ºC.

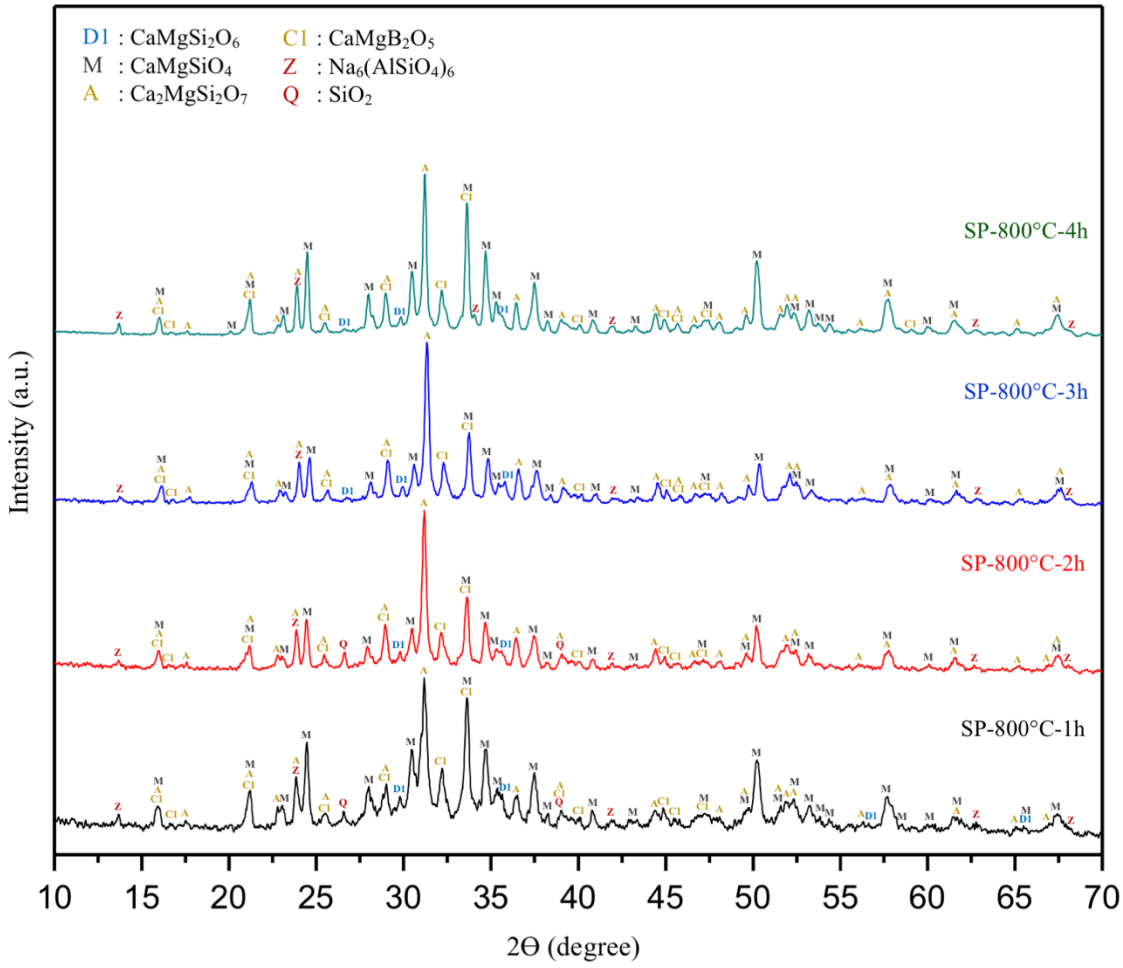

Figure 7.9. *Comparative XRD patterns of synthesized powders at 800°C for 1h, 2h, 3 h and 4 h*

Considering the XRD patterns in Fig. 7.8. and Fig. 7.9. nucleation and crystallization of calcium magnesium borate, akermanite and monticellite had already occurred until reaching 800°C. The crystal growth of these phases kept on with the increment of dwell time. It is deducible from gradually decreasing FWHM values at 800°C from 1 minute to 4 hours. Concordantly, amorphous condition considerably diminished for longer dwell time than 1 hour. In addition, peak shifting was observed for akermanite and monticellite phases especially for SP-800°C-3h and SP-800°C-4h specimens due to lattice distortion [78]. That can be caused by macroscopic residual compressive stress resulting from quenching in air and stress fields induced by the porosities and/or vacancies in the grain boundaries [85].

Fig. 7.10. illustrates the mass change graph for obtained powders after synthesis. Although, the equal mass of boron derivative waste (10 g) as a raw material used for each thermal process, the mass of obtained powders shows variability. The mass ranges of synthesized powders at 650°C and 800°C are 6.4 - 8.5 g and 6.2 - 6.6 g. The obtained results show that powder mass is decreasing with the increment of dwell time from 1 min to 4 h for each heat treatment temperature or with the increasing of temperature from 650°C to 800°C for stable dwell time (1 min) because higher temperature and/or longer dwell time makes thermal decomposition reactions of dolomite and calcite more thermodynamically and kinetically favored. The complete calcination of dolomite at 650°C between 1 min and 1 hour leads to highest mass change. SP-800°C-4h sample possesses lowest mass (6.2 g) following to dolomite and calcite decomposition.

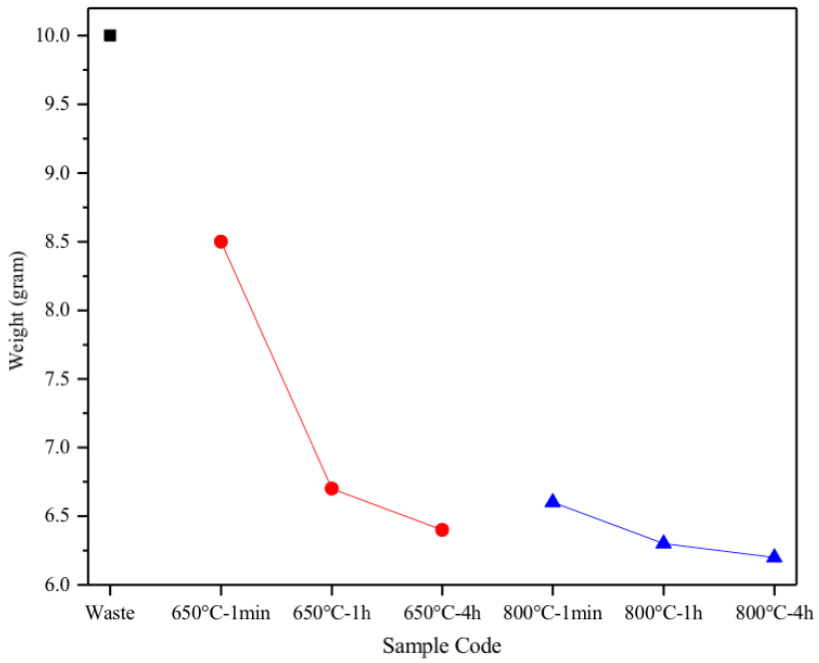

Figure 7.10. *Mass change graph for obtained powders after synthesis*

To emphasize the important process parameters for phase decompositions and formations, dolomite was calcined by heat treatment at 650°C for 1 h or at 800°C for 1 min. Calcite disappeared after the thermal process at 800°C for 30 min. Both diopside and monticellite started to form under same process parameters: at 650°C for 30 min, at 800°C for 1 min and at 900°C for 1 min. Also, the formation of akermanite was observed firstly both at 800°C for 1 min and at 900°C for 1 min. In other words,

heat treatments at 650°C under 1 atm is not thermodynamically favored for akermanite formation in this system.

The formation ability of high temperature phases (diopside, monticellite, akermanite and forsterite) at lower temperatures compared to studies in literature was an interesting point encountered during the study. For instance, monticellite could be formed minimum at 650°C which has a stability region between 1450°C and 1500°C according to the ternary phase diagram (CaO-MgO-SiO_2) given in Fig. 7.11. [86].

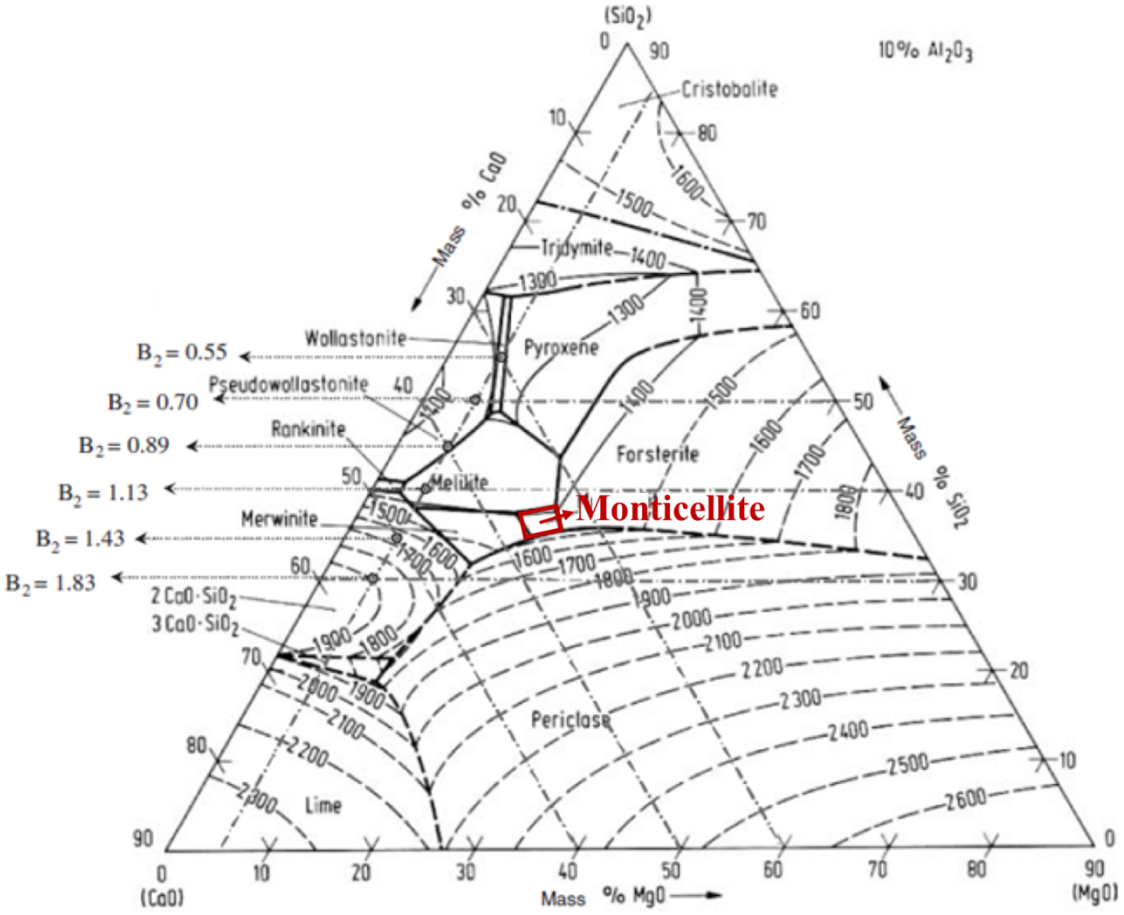

Figure 7.11. *Ternary phase diagram of CaO-MgO-SiO_2 system*

At lower temperatures and in shorter dwell times than predicted, the reasons to be able to provide formation and decomposition of phases in this work;

• The using of boron derivative waste as starting material in low mass (10 g) and refractory basement with large surface area (10 x 10 cm^2). In other words, the high surface area of refractory basement per unit of waste mass.

• The using of furnace pipe in order to facilitate CO_2 gas discharge which increases the partial pressure of CO_2 on the surface.

• The decreased viscosity and increased diffusion in results of the high amount of fluxing agents (Na_2O, B_2O_3, MgO and CaO) come from borax pentahydrate, dolomite and calcite [87,88].

7.3.2. Microstructure analysis of boron derivative waste and synthesized powders

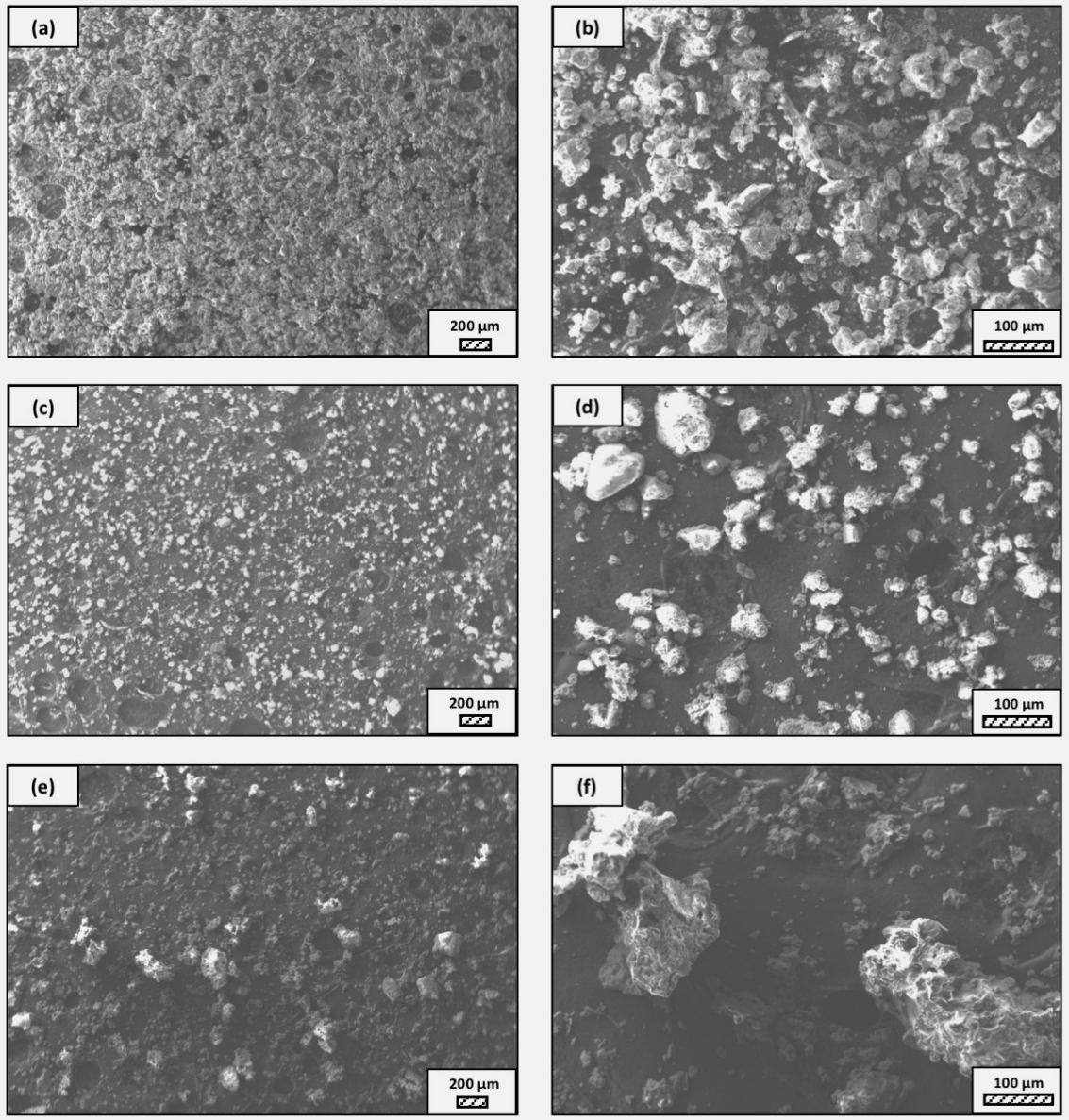

Figure 7.12. *SEM images (SE mode) of boron derivative waste (a, b); SP-650°C-4h (c, d) and SP-800°C-4h (e, f) at equal magnifications (100x and 500x)*

The SEM images (SE mode) of boron derivative waste, SP-650°C-4h and SP-800°C-4h are given in Fig. 7.12. SEM images indicates that boron derivative waste is comprising clusters which are composed of fine particles in non-spherical morphology. In comparison of SP-650°C-4h with SP-800°C-4h, both powder is consisted of non-equiaxial particles while the mean particle size of SP-800°C-4h is higher. It is stated that the increasing of temperature causes Ostwald ripening where small particles tend to dissolve and large particles grow [89].

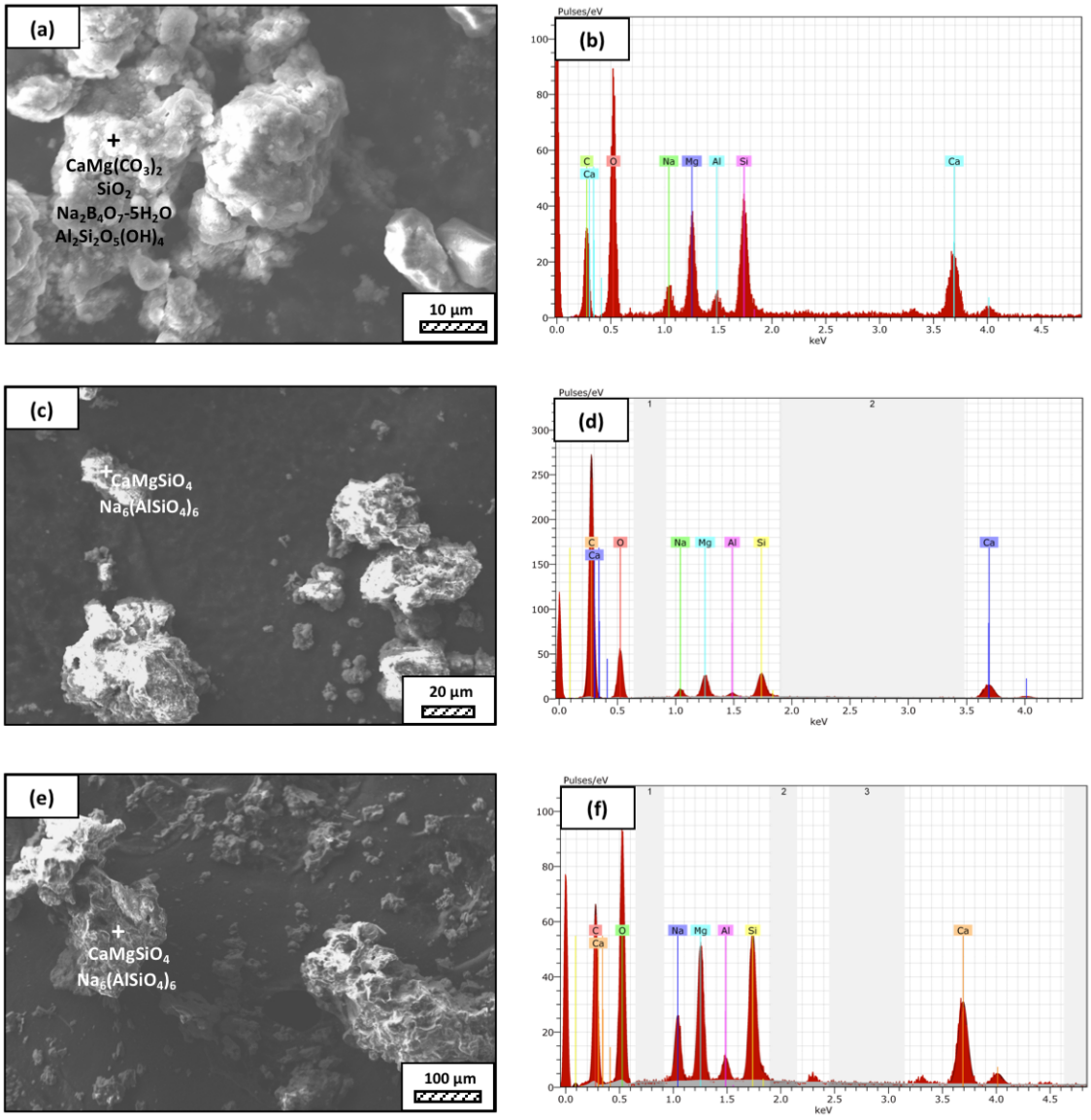

Figure 7.13. *SEM images (SE mode) and EDX spectrums of boron derivative waste (a, b); SP-650°C-4h (c, d) and SP-800°C-4h (e, f)*

SEM images (SE mode) and EDX spectrums of boron derivative waste, SP-650°C-4h and SP-800°C-4h are illustrated in Fig. 7.13. Confirming the XRD patterns, the results of semi-quantitative analysis point out the existing of dolomite, quartz, borax pentahydrate and kaolinite in boron derivative waste. Also, both SP-650°C-4h and SP-800°C-4h includes monticellite and zeolite particles. It is observed that the clusters are formed in synthesized powders which are composed of particles with different compositions, and the primary particles are located on the surface of clusters. It could be caused by complex system where alkali and alkaline metal oxides reacts with quartz as dominant phase within the same micro-locations.

7.4. Particle Size Reduction of Monticellite Based Ceramic Powder

To investigate the effect of particle size on bone-like apatite formation ability of monticellite based ceramic powders, SP-800°C-4h was crushed and milled prior to *in vitro* bioactivity assessment. The reason of using SP-800°C-4h lies its crystalline phases such as monticellite, akermanite, diopside, calcium magnesium borate and zeolite. Monticellite, akermanite and diopside have already known as biocompatible and bioactive ceramics. *In vitro* studies exhibited that nano-sized LTA zeolites does not create significant cytotoxic activity on macrophages, epithelial and endothelial cells for doses up to 500 μg / mL for 24 h. Due to their stability in biological environments, nano-zeolites have a potential to be used in different applications such as biosensors, controlled drug delivery, controlled gas delivery, magnetic resonance and fluorescent imaging agents and cosmetics [90]. In addition, calcium magnesium borate may improve the biocompatibility of monticellite based ceramic powder due to boron dissolution. It is stated that a beneficial interaction occurs between boron and steroid hormones involved in bone metabolism, and boron may also help prevent to bone-related diseases such as osteoporosis, arthritis and other steroid hormone dependent diseases [91]. Moreover, Pizzorno expressed the anti-inflammatory effects of boron which can help alleviate arthritis and improves brain function. Boronated compounds are now being used in the treatment of several types of cancer [92]. Hence, the obtaining of monticellite based ceramic powder from a boron waste can improve the biological properties of produced bone graft substitutes and may present new perspectives about different applications.

Milling is preferred in order to obtain a particular particle size distribution. In the planetary ball mill, the bowl and the supporting disk rotate in opposite direction

and centrifugal force produced by the vials which consists the powder and balls. The centrifugal force triggers the balls to move along the vial wall. The balls hit the particles and thus liberates massive impact momentum. In this way, crushing and milling are carried out by shear forces. Along with the fracture of a solid, energy as heat is released from fracture and it is necessary for creating additional surface area [93-95].

The particle size distribution and the degree of disorder of milled powders depend on the milling conditions such as the materials of milling tools, milling speed, milling time, milling environment and ball-to-powder weight ratio [96]. Dry milling could avoid the formation of hard agglomerates. Using milling media composed of hard materials maximizes the milling efficiency and consequently, minimizes the milling time to obtain fine powder. However, this case causes contamination in result of ball's wear. The materials of milling tools preferred ZrO_2 due to its biocompatibility and bioinert characteristics, high fracture toughness (brittleness), fairly high Vickers hardness (12.5 GPa) and high density (5.9 g/cm^3) [32,91,93]. The milling speed (400 rpm), milling environment (dry) and ball-to-powder weight ratio (10:1) kept constant whereas milling time increased from 1 h to 4 h with 1 h time intervals. During dry milling, the powder can cake onto the sides of the bowl and further size reduction is no more received [90]. In order to reduce this caking problem, the direction of rotation of the planetary ball mill was reversed and the sides of the bowl were scraped down per hour. Also, stearic acid added in this purpose as a deflocculant in 1 wt.% of charged powder.

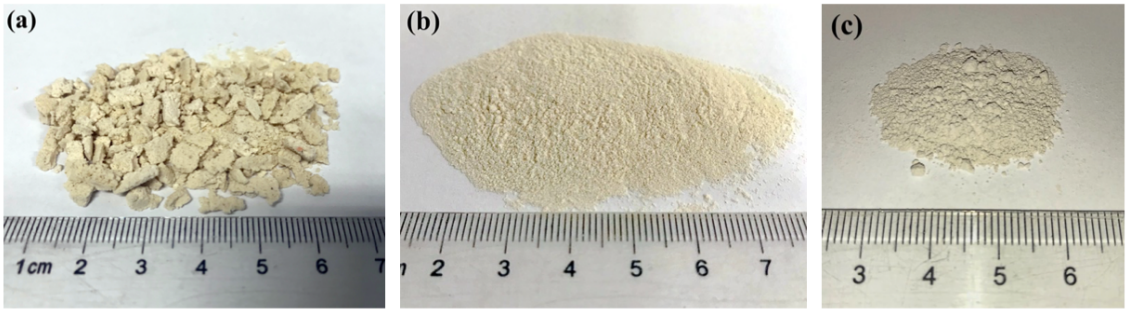

Figure 7.14. Images of a) synthesized powder at 800°C for 4 h (SP-800°C-4h), b) crushed SP-800°C-4h and c) ball-milled SP-800°C-4h for 2 h

Table 7.4. Three characteristic particle diameters of crushed & ball-milled monticellite based ceramic powders

Sample Code	d(0.1) µm	d(0.5) µm	d(0.9) µm
SP-800°C-4h-crushed	0.567	3.091	42.856
SP-800°C-4h-milled-1h	0.604	1.517	5.216
SP-800°C-4h-milled-2h	0.574	1.463	4.813
SP-800°C-4h-milled-3h	0.618	1.621	5.481
SP-800°C-4h-milled-4h	0.603	2.002	8.894

Images of synthesized powder at 800°C for 4 h (SP-800°C-4h), crushed SP-800°C-4h in an agate mortar and ball-milled SP-800°C-4h for 2 h are given in Fig. 7.14. Three characteristic particle diameters of crushed SP-800°C-4h and ball-milled SP-800°C-4h for 1, 2, 3 and 4 h determined by laser diffraction particle size analysis are given in Table 7.4. The crushed powder was composed of particles in a broad size range of 0.5 - 42.8 µm with an average size of 3.0 µm. After ball-milling of crushed powder for 1 h, particle size range was narrow (0.6 - 5.2 µm) and the mean particle size decreased from 3.0 µm to 1.5 µm. With the increasing of milling time from 1 h to 2 h, particle size range became narrower (0.5 - 4.8 µm) and the decreasing of mean particle size went further (1.4 µm). However, the ball-milling for more than 2 h was inefficient to decrease the particle size range. The particle size range of SP-800°C-4h-milled-3h was found (0.6 - 5.4 µm) and also, d50 value slightly increased to 1.6 µm due to agglomeration of particles. A noticeable broadening in particle size range of SP-800°C-4h-milled-4h (0.6 - 8.8 µm) was observed. Furthermore, ball-milling for 4 h caused a remarkable increment in the mean particle size (2.0 µm). Due to the agglomeration of particles with ball-milling for more than 2 h, the optimal milling time was selected 2 h in order to obtain the finest monticellite based ceramic powder.

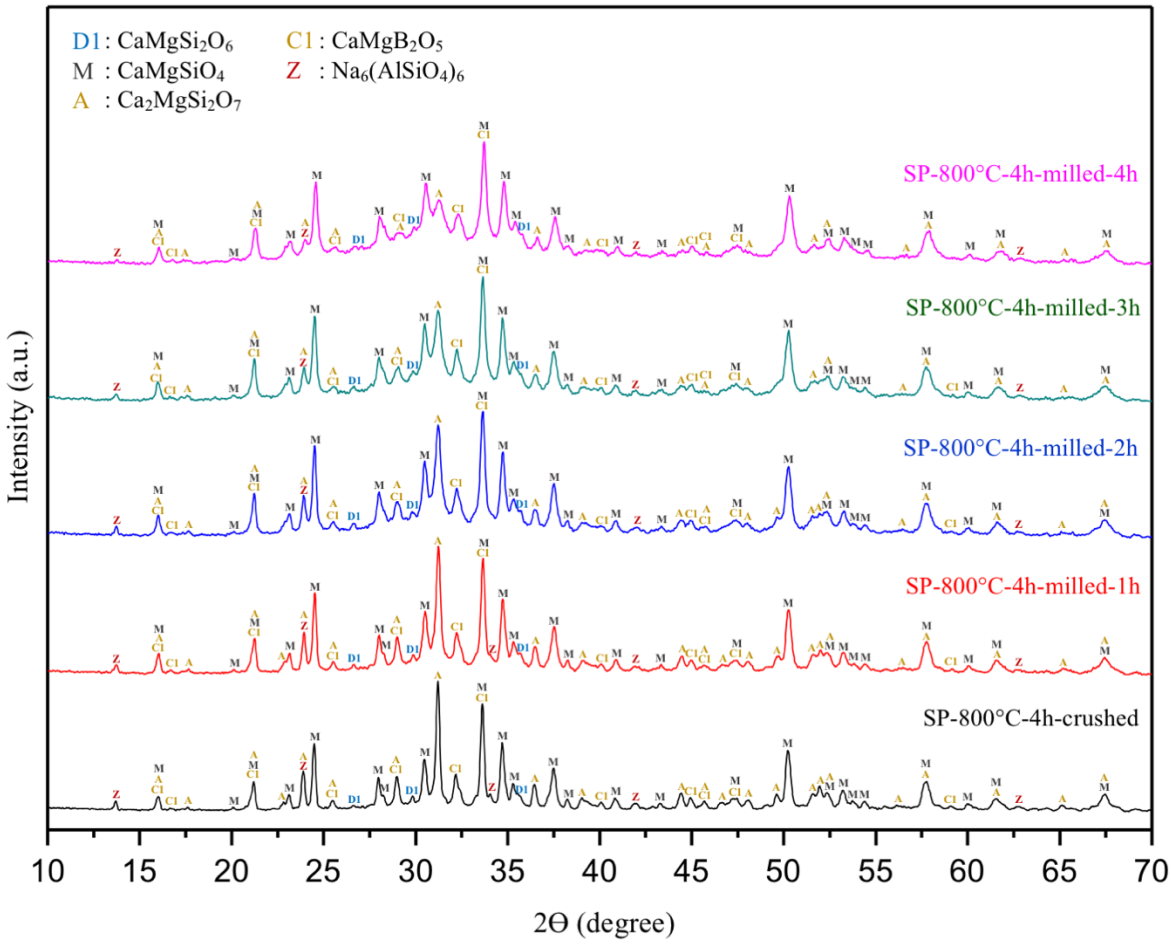

Figure 7.15. *Comparative XRD patterns of crushed SP-800°C-4h and ball-milled SP-800°C-4h for 1, 2, 3 and 4 h*

There is no more fast and easy way to get quick information on the milling progress than XRD that exposes the mean structural changes upon ball-milled powders for different milling times [96]. Comparative XRD patterns of crushed SP-800°C-4h and ball-milled SP-800°C-4h for 1, 2, 3 and 4 h are given in Fig. 7.15. In similarly to SP-800°C-4h, crushed and all milled powders include same crystalline phases such as monticellite, akermanite and calcium magnesium borate in substantially and also, diopside and zeolite. It indicates that there is no contamination of ZrO_2 through milling media and no newly formed crystalline phases. Although XRD patterns of crushed SP-800°C-4h and milled SP-800°C-4h for 1 h are very similar, the peak intensities of akermanite relatively decreased for milled SP-800°C-4h for 2 h and this manner went further with the increment of milling time from 2 h to 4 h as indication of enhancing of the amorphous content. Akermanite passed from its starting long-range ordered structure to short-range ordered structure with repeated collisions. It is interesting that

the amorphization was observed in akermanite while not in monticellite. It is attributed to the lower Mg/Ca ratio of akermanite (0.5) than that of monticellite (1). Mg-O bond energy was higher than that of Ca-O bond. Thus, higher MgO content makes the crystal structure more stable [28,34]. Therefore, in contrast to monticellite, milling impact was able to affect the stability and crystallization of akermanite by breaking down its crystal structure. In addition, both ball-milling compared to crushing and the increasing of ball-milling time led to enhancement in FWHM values of major phases (monticellite, akermanite, calcium magnesium borate), confirming the decreasing of crystallite sizes. Considering the particle diameters in Table 7.4., the mean particle size of ball-milled powders no more decreased after 3 h even if the crystallite sizes of major phases decreased with milling time according to XRD patterns. It points out that amorphization of akermanite and high milling times caused the formation of larger particles by agglomeration which are composed of crystallites in lower sizes.

7.5. Bone-Like Apatite Formation Ability of Monticellite Based Ceramic Powders

In the scope of assessment of *in vitro* bioactivity, the monticellite based ceramic powder wafers were prepared using crushed SP-800°C-4h and ball-milled SP-800°C-4h for 2 h. The investigation of the effect of particle size on bone-like apatite formation ability of monticellite based ceramic powders was one of the main aims of the present study. Hence, the reason for choosing ball-milled SP-800°C-4h for 2 h lies on its narrowest particle size range and lowest mean particle size in ball-milled monticellite based ceramic powders.

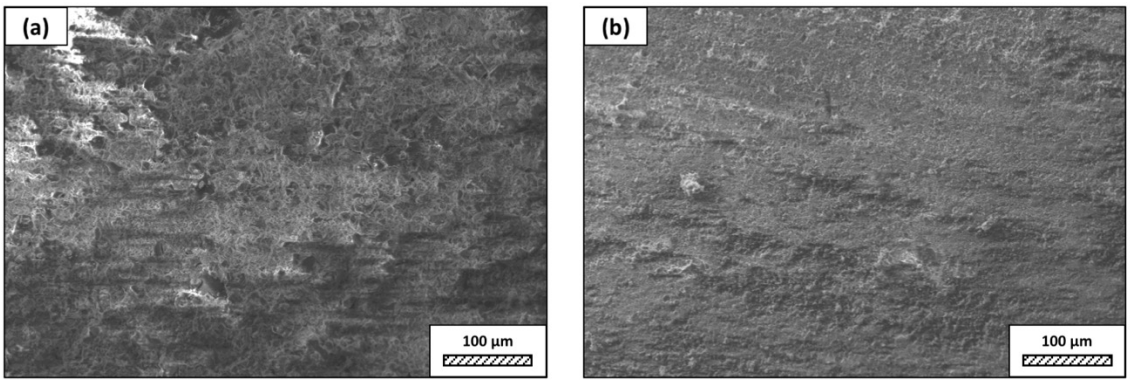

Figure 7.16. *SEM images (SE mode) of wafer surfaces composed of crushed SP-800°C-4h (a) and SP-800°C-4h-milled-2h (b) before incubation at equal magnification (500x)*

SEM images (SE mode) of the surfaces of crushed SP-800°C-4h wafer and SP-800°C-4h-milled-2h wafer before incubation are given in Fig. 7.16. at equal magnification (500x). As stated above, there is a difference in the particle size range and mean particle size of crushed and milled powders. During pelletization by dry uniaxial pressing, especially particle size range affects the packing and alters the surface characteristics such as roughness and surface area per volume [89]. It is reported that the larger specific surface area provides faster release of ions and higher protein absorption due to high surface energy per volume, which improves bioactivity [97]. According to Fig. 7.16., the surface of SP-800°C-4h-milled-2h wafer is smoother and its specific surface area is higher compared to crushed SP-800°C-4h wafer due to smaller particles. For this reason, it is expected the bioactivity of milled powder would be improved.

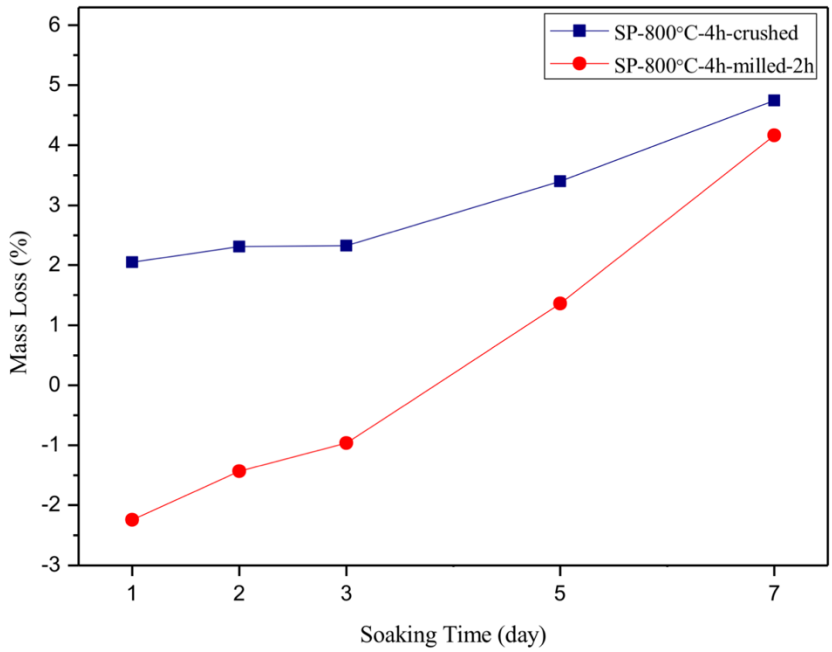

Figure 7.17. *Mass loss (%) values of wafers with respect to soaking time*

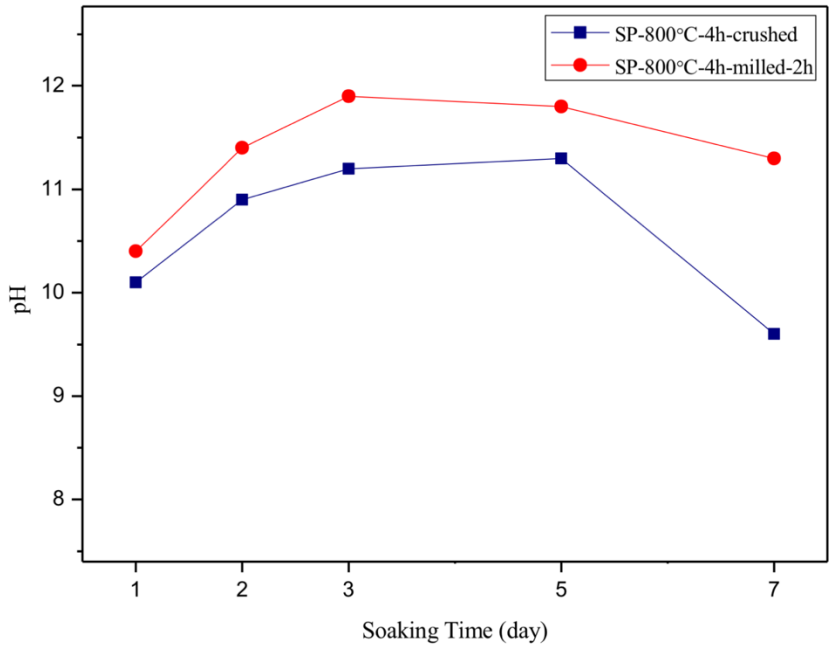

Figure 7.18. *pH values of Lac-SBF with respect to soaking time*

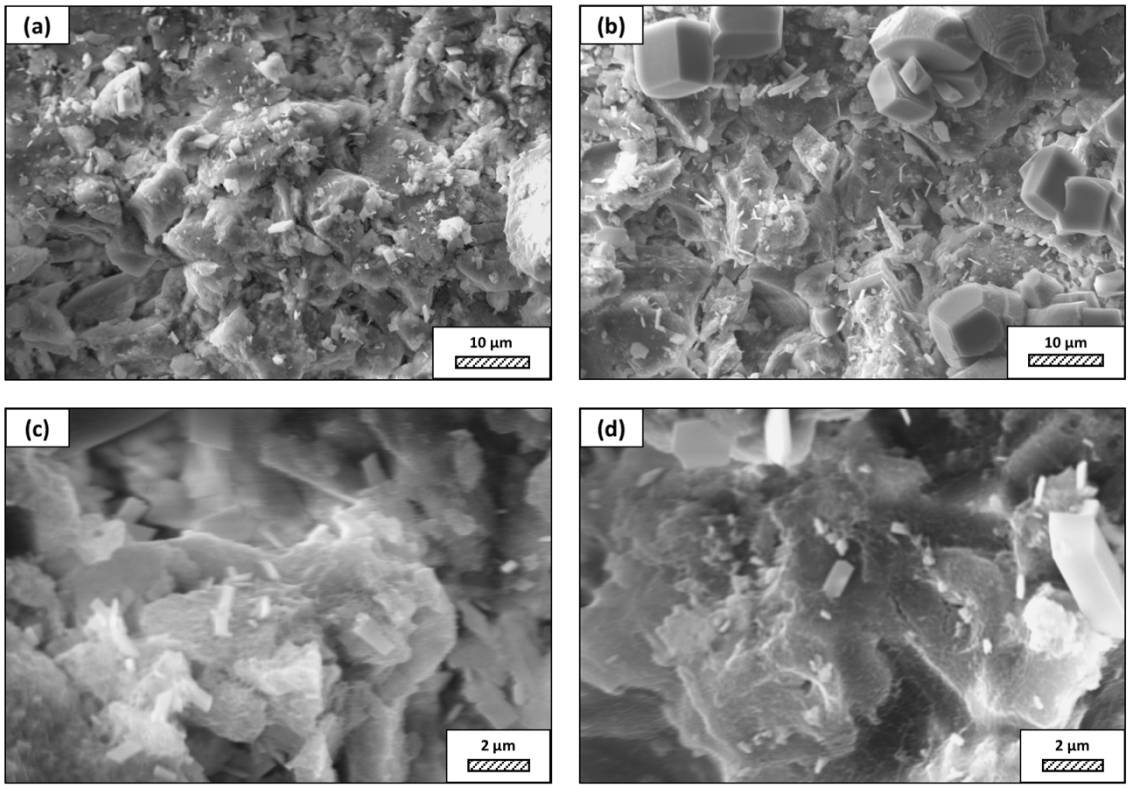

Figure 7.19. *SEM images (SE mode) of crushed SP-800°C-4h wafer (a, c) and SP-800°C-4h-milled-2h wafer (b, d) soaked in Lac-SBF for 7 days at equal magnifications (5.000x and 20.000x)*

The mass loss (%) values of wafers and pH values of Lac-SBF with respect to soaking time are given in Fig. 7.17. and Fig. 7.18. SEM images (SE mode) of crushed SP-800°C-4h wafer and SP-800°C-4h-milled-2h wafer (b, d) soaked in Lac-SBF for 7 days are illustrated in Fig. 7.19. According to Fig. 7.17. and Fig. 7.18., pH values of Lac-SBF increased from 7.4 to above 10 for both wafers after immersion for 1 day. In the first three days of incubation, pH values of Lac-SBF enhanced to above 11 for both wafers as a result of the exchange of alkali ions with hydrogen ions from Lac-SBF as the first step of bioactivity mechanism [11,32,33]. On the 3rd day of immersion, mass loss of crushed SP-800°C-4h wafer (coarse wafer) was 2.32 % whereas mass gain of SP-800°C-4h-milled-2h wafer (fine wafer) had still been continued. It is attributed to the higher specific surface area & higher surface energy of SP-800°C-4h-milled-2h wafer which provide higher ion absorption. On the 4th day of immersion, the SP-800°C-4h-milled-2h wafer started to lose mass, too. The mass loss of crushed wafer reached to 4.74 % and that of fine wafer increased to 4.16 % with the soaking of 7 days. Following to incubation of 3 days for the fine wafer and immersion for 5 days for the coarse wafer, pH values decreased from 11.9 to 11.3 and from 11.3 to 9.6 up to 7 days, respectively. The decreasing of pH of Lac-SBFs and the increasing of mass loss for both wafers are related with the network dissolution by breaking the Si-O-Si bonds, polymerization of the SiO_2-rich layer with the condensation of silanol (SiOH) groups and consequently, the formation of a $CaO-P_2O_5$ rich film onto the surface of silica-rich layer. In the comparison of crushed SP-800°C-4h wafer and SP-800°C-4h-milled-2h wafer, the fine wafer gained mass, its total mass loss was lower and pH values were higher during the test due to its higher specific surface area. The pH value for fine wafer started to decrease before points out the faster bioactivity mechanism compared to the coarse wafer.

During microstructural analysis of crushed SP-800°C-4h wafer and SP-800°C-4h-milled-2h wafer soaked in Lac-SBF for 7 days, the primary particles and newly formed thin layer on the surface of synthesized powders are observed. In addition, Ca/P ratio was determined using EDS detector. The spot analysis was performed on different locations of wafer surface. According to obtained results, mean atomic concentration of phosphor increased from 2.88 to 4.76 % for crushed SP-800°C-4h wafer and from 3.37 to 7.28 % for SP-800°C-4h-milled-2h wafer with the immersion for 7 days. Both the increasing of P content and the surface morphology of wafers indicates

the bone-like apatite formation ability of monticellite based ceramic powders as a sign of bioactivity characteristic. The mass loss behavior, the alteration manner of pH values of Lac-SBF and higher P content for SP-800°C-4h-milled-2h wafer soaked in Lac-SBF for 7 days shows that the particle size reduction creates a positive effect on the bone-like apatite formation ability of monticellite based ceramic powders. The obtaining of very high Ca/P ratio could be caused by small crystallite sizes of newly formed bone-like apatite layer and also high interaction volume during EDX analysis. It is important to state that it is an ongoing study and to proceed *in vitro* bioactivity tests up to 21 days is still necessary to make right comments.

7.6. The Effect of Monticellite Based Ceramic Powder on Cell Viability

In order to assess the biological performance, monticellite based ceramic powder (MBCP) was used which had been synthesized at 800°C for 1 h during preliminary study of this thesis. MBCP is consisted of crystalline phases such as monticellite, akermanite, diopside and calcium magnesium borate. The effect of coarse MBCP on cell viability was studied by using MTT and NRU protocol. MTT assay is based on the reduction of yellow dye (MTT), to purple formazan crystals by mitochondrial dehydrogenase activity, only present in metabolically active cells [61]. NRU assay is based on the ability of viable cells to incorporate and bind neutral red (NR), a supravital dye [62].

Determination of cytotoxicity can be realized by qualitative or quantitative evaluations. It is stated in ISO 10993-5 standard that for the qualitative evaluations such as MTT and NRU protocols, if the reduction of cells is not more than 20 %, material has slight cytotoxicity; no more than 50 % in cell reduction refers mild cytotoxicity; more than 50 % in cell reduction means moderate cytotoxicity; and nearly complete destruction of cells points out severe cytotoxicity.

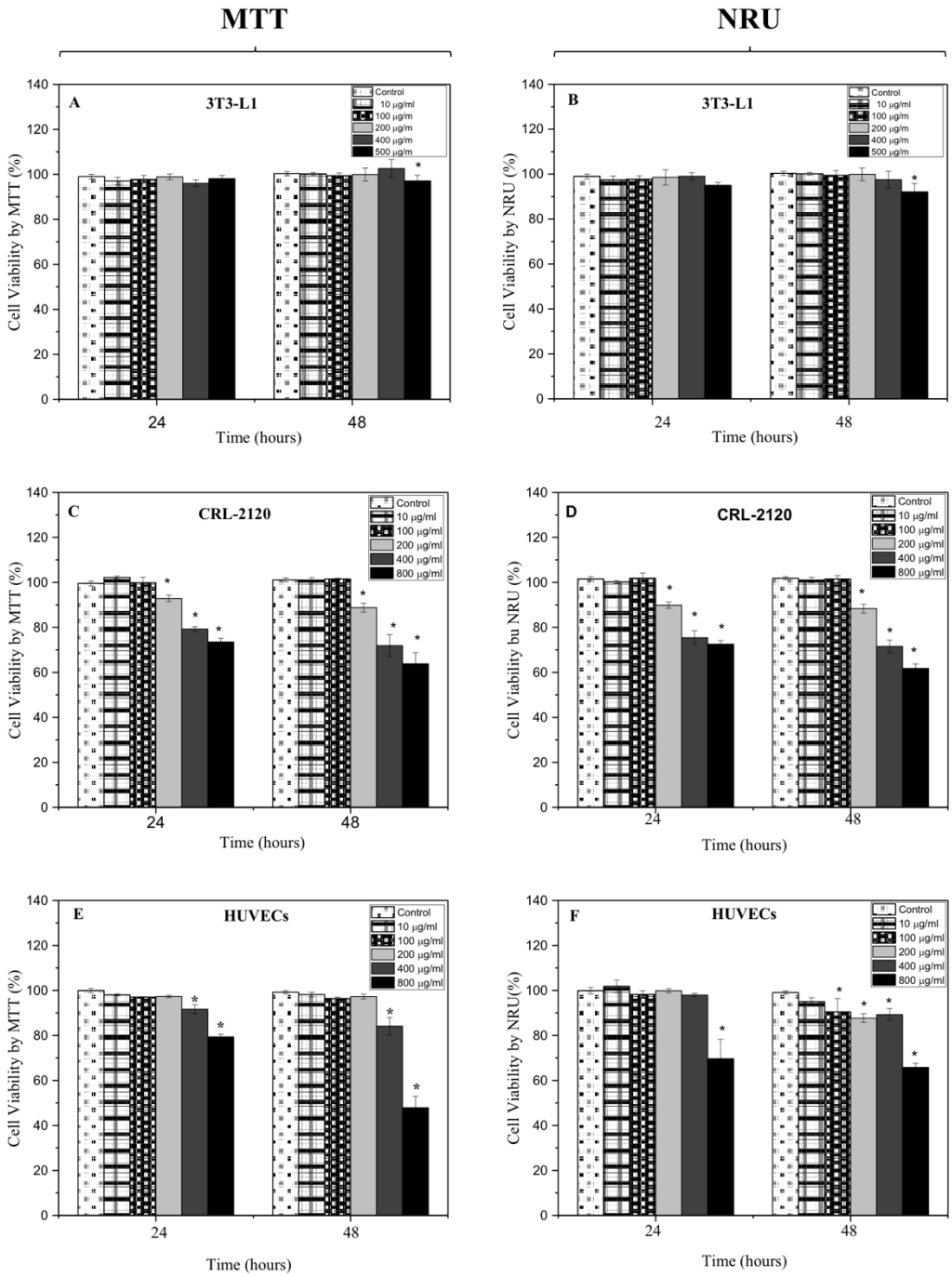

Figure 7.20. *Effects of monticellite based ceramic powder on the viability on 3T3-L1 cells (a-b), CRL 2120 cells (c-d), HUVECs (e-f) as determined by MTT and NRU respectively. Powder treatment for 24 and 48 h, values are means ± SD of triplicates. Asterisks (*) represent means significant difference from the control group by the Tukey test ($p<0.05$).*

Quantification of metabolically active cells was performed for two-time points by means of the MTT and NRU assays. Cells were treated with different concentrations of monticellite based ceramic powder for 24 - 48 h and results of which are presented

in Fig. 7.20. According to MTT results, 3T3-L1 cell viability was remained same as the control group at the concentrations of MBCP in the assessed range (10-800 µg/ mL) after 24 and 48 h (Fig. 7.20. (a)). Similarly, to the MTT results, it was found that monticellite based ceramic powder has no cytotoxicity at the concentration range 10 - 400 µg/ mL and has slight cytotoxicity at 800 µg/ mL concentration on 3T3-L1 cell viability in NRU assay (Fig. 7.20. (b)). The effect of MBCP on the viability of another fibroblast cell line, CRL 2120, was also examined and compared to 3T3-L1 cells. At the concentration range 10 - 100 µg/ mL of the test material, the cell viability values were almost the same with the control group in MTT and NRU assays. Cell viability of CRL 2120 cells decreased to 85 % at the higher concentration (200 µg/ mL) of MBCP on the first day. The results of the MTT and NRU assays showed that the significant reduction in the cell viability observed at the highest concentration (800 µg/ mL), cell viability decreased approximately 27 % on the first day and 37 % on the second day. According to MTT results, cytotoxic effects of MBCP in HUVECs were shown in Fig. 7.20. (e). HUVECs viability was remained same with the control group at the concentrations of MBCP in the assessed range (10 - 200 µg/ mL) after 24 and 48 h (Fig. 7.20. (e)). At the concentration range of 400 and 800 µg/ mL of the test material, there was no significant decrease (6 % and 14 %) on the first day in cell viability on HUVECs. Similarly, cell viability decreased 16 % on the second day on HUVECs at the concentration of 400 µg/ mL of the test material. The results obtained from both MTT and NRU assay showed that monticellite based ceramic powder has no cytotoxicity at the concentration range 10 - 200 µg/ mL and has slight cytotoxicity at 400 µg/ mL concentration on the first day (Fig. 7.20. (e-f)). The maximum cell death (53 %) was shown at the highest concentration (800 µg/ mL). The IC50 values of MBCP in HUVECs were 745 µg/ mL in MTT assay. According to NRU results, cytotoxic effects of MBCP in HUVECs were shown in Fig. 7.20. (f). At the concentration range 10 and 400 µg/ mL of the test material, there was no significant decrease (3 % - 5 %) on the first day in cell viability on HUVECs. A significant effect (64 %) was observed on the viability on HUVECs at the highest concentration (800 µg/ mL). The IC50 level was not reached in HUVECs by NRU assay. Similarly, IC 50 values were not reached in CRL 2120 and 3T3-L1 cells.

7.7. The Effect of Monticellite Based Ceramic Powder on the Mitochondrial Membrane Potential

The membrane-permeant JC-1 dye is widely used in apoptosis studies to monitor mitochondrial health. The lipophilic cation JC-1 was used to assess the mitochondrial status of CRL2120 cells against crushed SP-800°C-4h. According to the manufacturer (Molecular Probes, Eugene, OR, USA), JC-1 changes reversibly its fluorescence. When the mitochondrial membrane potential is high orange fluorescence exist in the green cytosol (multimeric status). If there is the loss of the mitochondrial membrane integrity, it is only green fluorescence [98].

Concentrations of the test material (50 μg/ mL, 100 μg/ mL, 200 μg/ mL, 400 μg/ mL and 800 μg/ mL) were performed on CRL 2120 cells for 24h. After the incubation and dye process slides were investigated under the fluorescence microscope in-depth to analyze the dose-dependent mitochondrial membrane changes. Fig. 7.21. demonstrates representative JC-1 stains of CRL 2120 cells. All slides at the concentration range 10 and 200 μg/ mL of the test material gave quite a bright orange fluorescence as well as control group (Fig. 7.21.), which means that there is no significant decrease in mitochondrial membrane potential, but the potential changed after treatment with the concentration range 400 and 800 μg/ mL of monticellite based ceramic powder. The cell cytosol color changed red to green as a sign of a cytotoxic effect. This indicated that apoptosis might have occurred at the highest concentration (800 μg/ mL) of monticellite based ceramic powder.

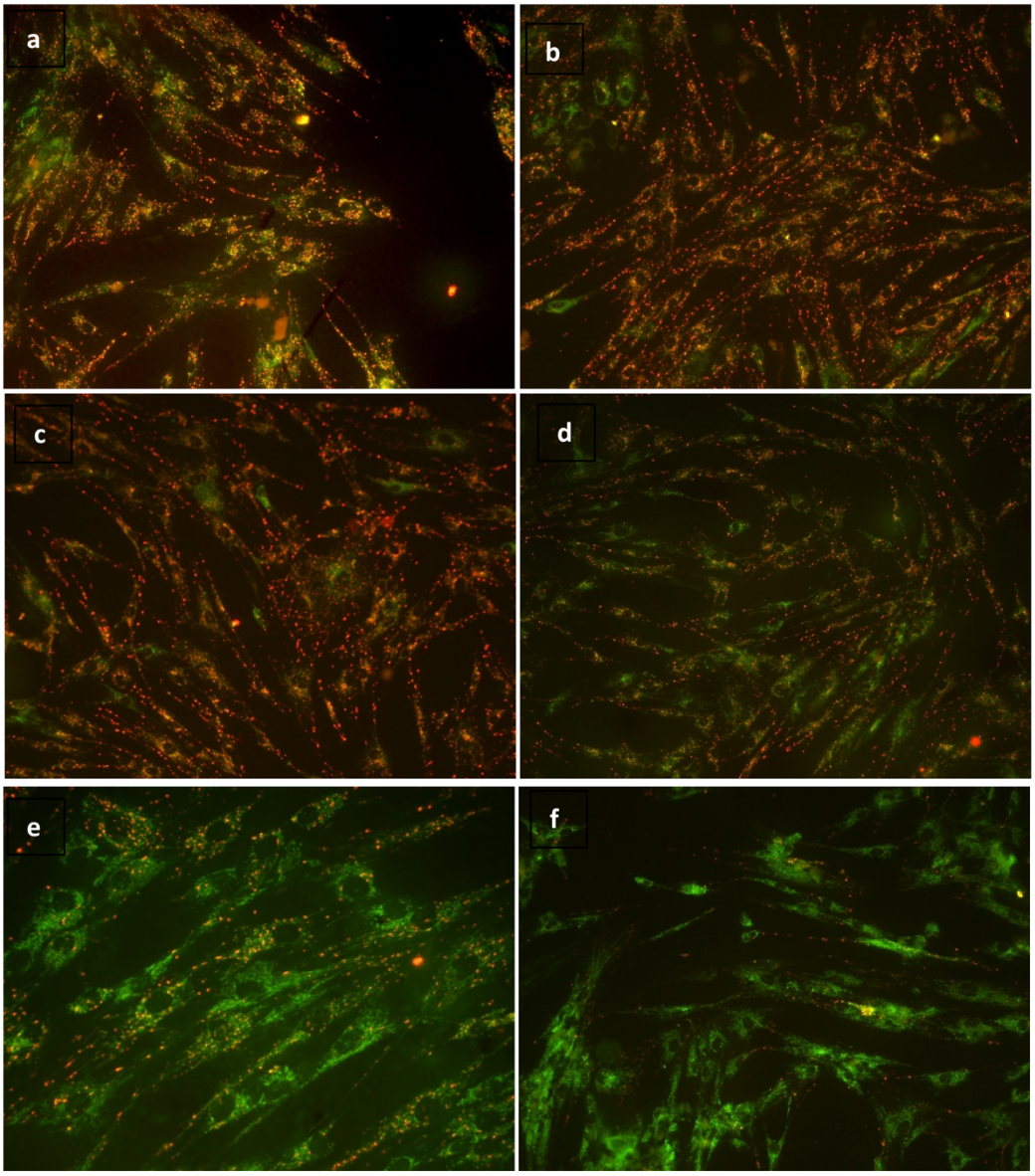

Figure 7.21. *Effects of monticellite based ceramic powder on mitochondrial membrane potential in CRL 2120 cells. a) Control, b) 50 µg/ mL, c) 100 µg/ mL, d) 200 µg/ mL, e) 400 µg/ mL and f) 800 µg/ mL. Images were taken using 10X objective lens.*

8. CONCLUSION

In this thesis work, a novel approach in a cost-effective and environmentally friendly way was presented for the synthesis of monticellite based bioactive ceramic powders from boron derivative waste. During the systematic heat-treatments of boron derivative waste at 650°C and 800°C for various dwell times between 1 min and 4 hours, carried out in the scope of investigation of phase transformation mechanism, monticellite phase could be formed at 650°C where it is stable at 1450°C according to

CaO-MgO-SiO_2 phase diagram. The most stable monticellite based ceramic powder was synthesized at 800°C for 4 h (SP-800°C-4h) and composed of monticellite, akermanite, diopside, calcium magnesium borate and zeolite crystalline phases. In order to investigate the effect of particle size on bone-like apatite formation ability of monticellite based ceramic powders, ball-milling time was optimized and then, both wafers composed of crushed SP-800°C-4h and ball-milled SP-800°C-4h for 2 h were soaked in Lac-SBF for 7 days. The increment of mass loss of wafers, the manner of pH alteration in Lac-SBFs, the formation of thin layer on the surface of synthesized powders and the increasing of phosphor content in wafers within the 7 days of immersion indicated the formation of bone-like apatite layer ability of monticellite based ceramics powders. Also, the obtained results showed that the particle size reduction accelerates the bioactivity mechanism of monticellite based ceramic powders. Nevertheless, to proceed *in vitro* bioactivity test up to 21 days is crucial for this ongoing study. In addition, the cytotoxicity of monticellite based bioactive ceramic powder, synthesized at 800°C for 1h from boron derivative waste during preliminary study of this thesis and composed of monticellite, akermanite, diopside and calcium magnesium borate phases, on different mammalian cell lines (3T3-L1, HUVEC, CRL-2120) was determined by in vitro assays of MTT, NRU and JC-1 staining at the concentrations of 10, 50, 100, 200, 400, 500 and 800 μg/ mL. The obtained results pointed out the biocompatible characteristic of monticellite based ceramic powder at the concentration range of 10 - 200 μg/ mL. The comprehensive *in vitro* studies based on the investigation of the effect of particle size on the biocompatibility of monticellite based ceramic powder will be conducted to assess its usage potential as a bone graft substitute for bone void filling and coating applications.

REFERENCES

[1] Polo-Corrales, L., Esteves, M.L. and Ramirez-Vick, J.E. (2014). Scaffold Design for Bone Regeneration. *J Nanosci Nanotechnol*, 14 (1), 15–56.

[2] Liang, W., Rahaman, M.N., Day, D.E., Marion, N.W., Riley, G.C., Mao, J.J. (2008). Bioactive borate glass scaffold for bone tissue engineering. *Journal of Non-Crystalline Solids*, 354 (15–16), 1690–1696.

[3] Korkusuz, F., Tomin, E., Yetkinler, D.N., Korkusuz, P. (2011). Synthetic bone grafts. *Journal of TOTBİD*, 10 (2), 134–142. (in Turkish).

[4] Nalla, R.K., Kruzic, J.J., Kinney, J.H., Balooch, M., Ager, J.W., Ritchie, R. O. (2006). Role of microstructure in the aging-related deterioration of the toughness of human cortical bone. *Materials Science and Engineering C*, 26 (8), 1251–1260.

[5] Henkel, J., Woodruff, M. A., Epari, D.R., Steck, R., Glatt, V., Dickinson, I.C., Choong, P.F.M., Schuetz, M.A., Hutmacher, D.W. (2013). Bone Regeneration Based on Tissue Engineering Conceptions - A 21st Century Perspectiand. *Bone Research*, 1 (3), 216–248.

[6] Orlovskii, V.P., Komlev, V.S. and Barinov, S.M. (2002). Hydroxyapatite and hydroxyapatite-based ceramics. *Inorganic Materials*, 38 (10), 973–984.

[7] Sadat-Shojai, M., Khorasani, M.T., Dinpanah-Khoshdargi, E., Jamshidi, A. (2013). Synthesis methods for nanosized hydroxyapatite with diverse structures. *Acta Biomaterialia*, 9 (8), 7591–7621.

[8] Roberts, T.T., Rosenbaum, A.J., Roberts, T.T., Rosenbaum, A.J., Roberts, T.T., Rosenbaum, A. J. (2016). Bone grafts, bone substitutes and orthobiologics Bone grafts, bone substitutes and orthobiologics: The bridge between basic science and clinical advancements in fracture healing, 8 (4), 114–124.

[9] Leach, K.J., Kaigler, D., Wang, Z., Krebsbach, P.H., Mooney, D.J. (2006). Coating of VEGF-releasing scaffolds with bioactive glass for angiogenesis and bone regeneration. *Biomaterials*, 27 (17), 3249–3255.

[10] Hafezi-Ardakani, M., Moztarzadeh, F., Rabiee, M., Talebi, A.R. (2011). Synthesis and characterization of nanocrystalline merwinite (Ca3Mg(SiO4)2) via sol-gel method. *Ceramics International*, 37 (1), 175–180.

[11] Salinas, A.J. and Vallet-Regí, M. (2013). Bioactive ceramics: from bone grafts to tissue engineering. *RSC Advances*, 3 (28), 11116.

[12] El-Meliegy, E. and Noort, R. Van. (2012). *Glasses and Glass Ceramics for Medical Applications*. New York: Springer-Verlag Publications.

[13] Boretos, J.W. and Eden, M. (1984). *Contemporary Biomaterials: Materials and Host Response, Clinical Application, New Technologies and Legal Aspects*. Park Ridge, NJ: Noyes Publications.

[14] Ratner, B. D. (2013). A History of Biomaterials. In *Biomaterials Science: An Introduction to Materials in Medicine* (p. 10-23). London: Elsevier Academic Press.

[15] Park, J. and Lakes, R.S. (2007). *Biomaterials: An Introduction*. New York: Springer-Andrlag.

[16] Parida, P., Behera, A. and Mishra, S.C. (2012). Classification of Biomaterials used in Medicine. *International Journal of Advances in Applied Sciences*, 1(3), 125-129.

[17] Hill D. (1998). *Design engineering of biomaterials for medical devices*. New York: Wiley.

[18] Patel, N. and Gohil, P. (2012). A review on biomaterials: scope, applications & human anatomy significance. *International Journal of Emerging Technology and Advanced Engineering*, 2 (4), 91–101.

[19] Maitra, S., Rahaman, A., Pyare, R., Mukhtar, H.B., Dutta., B.K. (2009). Synthesis and Characterization of Bioactive-Glass Ceramics. *Advances in Bioceramics and Porous Ceramics II.* 83-94.

[20] Heness, G. and Nissan, B.B. (2004). Innovative Bioceramics. *Materials Forum*, 27, 104-114.

[21] Hench, L.L. (1991). Bioceramics: From Concept to Clinic. *Journal of the American Ceramic Society*, 74 (7), 1487–1510.

[22] Baena, J., Wu, J. and Peng, Z. (2015). Wear Performance of UHMWPE and Reinforced UHMWPE Composites in Arthroplasty Applications: A Review. *Lubricants*, 3 (2), 413–436.

[23] Pasinli, A. and Aksoy, R.S. (2010). Yapay Kemik Uygulamaları İçin Hidroksiapatit. *Electronic Journal of BioTechnology,* 1 (111), 41–5141. (in Turkish).

[24] Koch, K., Brave, D. and Nasseh, A.A. (2013). A review of bioceramic technology in endodontics. *CE Article_bioceramic technology*, 10 (C), 6–13.

[25] Hench, L.L. (1992). Bioceramics: Research and Development Opportunities. *Brazilian Journal of Physics*, 22 (2), 70-84.

[26] Mordor Intelligence Comp. (2017). *Industry Report: Bioceramics Market - Global Analysis, Current Trends, Forecast to 2022.* India: Mordor Intelligence Press. https://www.mordorintelligence.com/industry-reports/bioceramics-market (Son Erişim Tarihi: 26.12.2017)

[27] Ahuja, A., Ahuja, V. and Singh, K.S. (2015). Current concepts of regenerative biomaterials in implant dentistry. *Journal of the International Clinical Dental Research Organization*, 7 (3), 34.

[28] Chen, X., Ou, J., Kang, Y., Huang, Z., Zhu, H., Yin, G., Wen, H. (2008). Synthesis and characteristics of monticellite bioactive ceramic. *Journal of Materials Science: Materials in Medicine*, 19 (3), 1257–1263.

[29] Pasinli, A., Yuksel, M., Celik, E., Sener, S., Tas, A.C. (2010). A new approach in biomimetic synthesis of calcium phosphate coatings using lactic acid-Na lactate buffered body fluid solution. Acta Biomaterialia, 6 (6), 2282–2288.

[30] Kokubo, T. and Takadama, H. (2006). How useful is SBF in predicting in vivo bone bioactivity?. *Biomaterials*, 27 (15), 2907–2915.

[31] Tas, A.C. (2014). Submicron spheres of amorphous calcium phosphate forming in a stirred SBF solution at 55°C. *Journal of Non-Crystalline Solids,* 400, 27–32.

[32] Santin, M. and Phillips, G. (2012). *Biomimetic, Bioresponsive, and Bioactive Materials: An Introduction to Integrating Materials with Tissues*. Hoboken, New Jersey: John Wiley & Sons, Inc.

[33] Hench, L.L. (2013). Chronology of Bioactive Glass Development and Clinical Applications. *New Journal of Glass and Ceramics*, 3 (2), 67–73.

[34] Chen, X., Ou, J., Wei, Y., Huang, Z., Kang, Y., Yin, G. (2010). Effect of MgO contents on the mechanical properties and biological performances of bioceramics in the MgO-CaO-SiO2system. *Journal of Materials Science: Materials in Medicine*, 21 (5), 1463–1471.

[35] Wu, C. and Chang, J. (2006). A novel akermanite bioceramic: Preparation and characteristics. *Journal of Biomaterials Applications*, 21 (2), 119–129.

[36] Huang, Y., Jin, X., Zhang, X., Sun, H., Tu, J., Tang, T., Chang, J., Dai, K. (2009). In vitro and in vivo evaluation of akermanite bioceramics for bone regeneration. *Biomaterials*, 30 (28), 5041–5048.

[37] Iwata, N.Y., Lee, G.H., Tsunakawa, S., Tokuoka, Y., Kawashima, N. (2004). Preparation of diopside with apatite-forming ability by sol-gel process using metal alkoxide and metal salts. *Colloids and Surfaces B: Biointerfaces*, 33 (1), 1–6.

[38] Ou, J., Kang, Y., Huang, Z., Chen, X., Wu, J., Xiao, R., Yin, G. (2008). Preparation and in vitro bioactivity of novel merwinite ceramic. *Biomedical Materials*, 3 (1).

[39] Diba, M., Goudouri, O.M., Tapia, F., Boccaccini, A.R. (2014). Magnesium-containing bioactive polycrystalline silicate-based ceramics and glass-ceramics for biomedical applications. *Current Opinion in Solid State and Materials Science*, 18 (3), 147–167.

[40] Wang, G.C., Lu, Z.F. and Zreiqat, H. (2014). Chapter 8: Bioceramics for skeletal bone regeneration. Mallick, K. (Editor), in *Bone Substitute Biomaterials* (p. 180-216). Cambridge: Woodhead Publishing.

[41] Deer, W.A., Howie, R.A., and Zussman, J. (1997). *Rock-forming minerals: volume 1A: orthosilicates.* London: Geological Society.

[42] Li, Y., Wang, Y., Xu, X., Yu, G., Zhang, F. (2010). Photoluminescence Properties and Valence Stability of Eu in CaMgSiO4. *Journal of The Electrochemical Society*, 157 (2), J39-J43.

[43] Gerhardt, L. and Boccaccini, A.R. (2010). Bioactive Glass and Glass-Ceramic Scaffolds for Bone Tissue Engineering. *Materials,* 3, 3867–3910.

[44] Wu, C., Chang, J., Wang, J., Ni, S., Zhai, W. (2005). Preparation and characteristics of a calcium magnesium silicate (bredigite) bioactive ceramic. *Biomaterials*, 26 (16), 2925–2931.

[45] Ridzwan, M.I.Z. (2007). Problem of Stress Shielding and Improvement to the Hip Implant Designs: A Review. *Journal of Medical Sciences*, 7 (3), 460-467.

[46] Kang, J.S., Moon, K.H., Kim, B.S., Kwon, D.K., Choi, J.M. (2012). Midterm Results of Total Hip Arthroplasty Using the VerSys Fiber Metal Tapered Femoral Stem. *Hip & Pelvis*, 24 (2), 79.

[47] Baad-Hansen, T., Kold, S., Olsen, N., Christensen, F., Søballe, K. (2011). Excessive distal migration of fiber-mesh coated femoral stems. *Acta Orthopaedica*, 82 (3), 308–314.

[48] Shamoradi, F., Emadi, R. and Ghomi, H. (2017). Fabrication of monticellite-akermanite nanocomposite powder for tissue engineering applications. *Journal of Alloys and Compounds*, 693, 601–605.

[49] Karadeniz, M. (1996). Cevher Zenginleştirme Tesis Artıkları, Çevreye Etkileri Önlemler. *İstanbul Ofset Basım Yayın*. (in Turkish).

[50] Cicek, B. (2013). Development of glass-ceramics from combination of industrial wastes with boron mining waste (Dissertation thesis). Alma Mater Studiorum, University of Bologna.

[51] Karasu, B., Kaya, G., Yurdakul., H. (2002). Effect of the etibor kırka borax company's concentration and derivation wastes on the properties of wall tile body. *Proceeding of the 1st International Boron Symposium, Kutahya, Turkey,* 224-228. (in Turkish).

[52] Uslu, T. and Arol, A.I. (2004). Use of boron waste as an additive in red bricks. *Waste Management,* 24, 217-220.

[53] Kavas, T. (2006). Use of boron waste as a fluxing agent in production of red mud brick, *Building and Environment,* 41 (12), 1779-1783.

[54] Christogerou, A., Kavas, T., Pontikes, Y., Koyas, S., Tabak, Y., Angelopoulos, G.N. (2009). Use of boron wastes in the production of heavy clay ceramics. *Ceramics International*, 35, 447-452.

[55] Elbeyli, I.Y. (2004). Utilization of industrial borax wastes (bw) for portland cement production. *Turkish J. Eng. Env. Sci.*, 28, 281-287.

[56] Över Kaman, D., Köroğlu, L., Ayas, E., Güney, Y. (2017). The effect of heat-treated boron derivative waste at 600 °C on the mechanical and microstructural properties of cement mortar. *Construction and Building Materials*, 154, 743–751.

[57] Kaur, G., Pickrell, G., Kimsawatde, G., Homa, D., Allbee, H., Sriranganathan, N. (2014). Synthesis, cytotoxicity, and hydroxyapatite formation in 27-Tris-SBF for sol-gel based CaO-P2O5-SiO2-B2O3-ZnO bioactive glasses. *Scientific reports*, 4, 4392.

[58] Wallin, R.F. (1998). *A Practical Guide to ISO 10993-12: Sample Preparation and Reference Materials*. London: Medical Device & Diagnostic Industry News Products and Suppliers.

[59] Marois, Y. and Guidoin, R. (2013). *Madame Curie Bioscience Database*. Austin (TX): Landes Bioscience.

[60] V.D.E.V. Gmbh, Ag, R.S. and Rechte, A. (2009). *International Standard ISO 10993-5: Biological evaluation of medical devices Part 5: Tests for in vitro cytotoxicity.* (3rd Edition). Geneva: International Organization for Standardization.

[61] Mossmann, T. (1983). Rapid colorimetric assay for cellular growth and survival: Application to proliferation and cytotoxicity assay. *Journal of Immunological, Methodology*, 65, 55-63.

[62] Borenfreund, E. and Puerner, J.A. (1985). A simple quantitative procedure using monolayer culture for cytotoxicity assays. *J. Tis. Cult. Meth.,* 9, 7-9.

[63] Castedo, M., Ferri, K., Roumier, T., Mètivier, D., Zamzami, N., Kraemer, G. (2002). Quantitation of mitochondrial alterations associated with apoptosis. *Journal of Immunological Methods*, 265, 39-47.

[64] Roos, P. M. (2014). Journal of Trace Elements in Medicine and Biology Osteoporosis in neurodegeneration. *Journal of Trace Elements in Medicine and Biology*, 28 (4), 418–421.

[65] Ferreira, J.M.D.F. and Goel, A. (2014). Bioactive glass composition, its applications and respective preparation methods. ABD, 20140193499 A1.

[66] Jung, S.B. and Day, D.E. (2011). Controlling calcium compound formation in biocompatible materials for tissue regeneration and repair in mammals. Avrupa, WO 2011084192 A1.

[67] Cvitas, T. (2007). The Gibbs function of a chemical reaction. *Croatica Chemica Acta*, 80 (3-4), 605–612.

[68] Cengel, Y.A. and Boles, M.A. (2002). *Thermodyamics: An engineering approach*. (5th Edition). New York: McGraw-Hill.

[69] Trindade, M. J., Dias, M. I., Coroado, J., Rocha, F. (2010). Firing tests on clay-rich raw materials from the algarve basin (Southern Portugal): Study of mineral transformations with temperature. *Clays and Clay Minerals*, 58 (2), 188–204.

[70] Sasaki, K., Qiu, X., Hosomomi, Y., Moriyama, S., Hirajima, T. (2013). Effect of natural dolomite calcination temperature on sorption of borate onto calcined products. *Microporous and Mesoporous Materials*, 171, 1–8.

[71] Mitchell, B.S. (2004). *An introduction to materials engineering and science: for chemical and materials engineers*. Hoboken, New Jersey: John Wiley & Sons, Inc.

[72] Kniess, C.T., Cardoso de Lima, J. and Prates, P.B. (2005). In Chapter 14: The quantification of crystalline phases in materials: Applications of Rietveld method. Shatokha, V. (Ed.). *Sintering - Methods and Products*. London: In Tech.

[73] Şahin, Ö. and Bulutcu, A.N. (2003). Evaluation of thermal decomposition kinetics of borax pentahydrate using genetic algorithm method by isothermal analysis. *Turkish Journal of Chemistry*, 27 (2), 197–207.

[74] Şahin, Ö. and Bulutcu, A.N. (2002). Dehydration Behaviour of Borax Pentahydrate to Anhydrous Borax by Multi-Stage Heating in a Fluidized. *Turkish Journal of Chemistry*, 26, 89–96.

[75] Cardelli, F. (2008). *Materials Handbook: A concise desktop reference.* (2nd Edition). London: Springer-Verlag.

[76] Maia, A.Á.B., Angélica, R.S., de Freitas Neves, R., Pöllmann, H., Straub, C., Saalwächter, K. (2014). Use of 29Si and 27Al MAS NMR to study thermal activation of kaolinites from Brazilian Amazon kaolin wastes. *Applied Clay Science*, 87, 189–196.

[77] Olszak-Humienik, M. and Jablonski, M. (2015). Thermal behavior of natural dolomite. *Journal of Thermal Analysis and Calorimetry*, 119 (3), 2239–2248.

[78] Cullity, B.D. and Stock, S.R. (1956). *Elements of X-Ray Diffraction*. (3rd Edition). Massachusetts: Addison-Wesley Publishing Company.

[79] Prokof'ev, V.Y. and Gordina, N.E. (2014). Preparation of granulated LTA and SOD zeolites from mechanically activated mixtures of metakaolin and sodium hydroxide. *Applied Clay Science*, 101, 44–51.

[80] Ríos, C.A., Williams, C.D. and Castellanos, O.M. (2010). Synthesis of zeolite LTA from thermally treated kaolinite. *Revista de la Facultad de Ingeniería*, 53 (53), 30–41.

[81] Rybakov, A.A., Bryukhanov, I.A., Larin, A.V., Zhidomirov, G.M. (2015). Carbonates in zeolites: Formation, properties, reactivity. *International Journal of Quantum Chemistry*, 115 (24), 1709–1717.

[82] Pisch, A., Ferey, F. and Briaud, V. (2012). Phase Equilibria and Thermodynamics in the CaO-Al2O3-B2O3 Ternary System in Air. *GTT Annual Workshop*.

[83] Monshi, A., Foroughi, M.R. and Monshi, M.R. (2012). Modified Scherrer equation to estimate more accurately nano-crystallite size using XRD. *World J. Nano Sci. Eng.*, 2 (3), 154.

[84] Colombo, P., Mera, G., Riedel, R., Soraru, G.D. (2010). Polymer-derived ceramics: 40 Years of research and innovation in advanced ceramics. *Journal of the American Ceramic Society*, 93 (7), 1805–1837.

[85] Qin, W., Nagase, T., Umakoshi, Y., Szpunar, J.A. (2007). Lattice distortion and its effects on physical properties of nanostructured materials. *Journal of Physics: Condensed Matter*, 19, 236217, 1-8.

[86] Chuang, H.C., Hwang, W.S. and Liu, S.H. (2009). Effects of Basicity and FeO Content on the Softening and Melting Temperatures of the CaO-SiO_2-MgO-Al_2O_3 Slag System. *Materials Transactions*, 50 (6), 1448–1456.

[87] Wang, H., Zhang, T., Zhu, H., Li, G., Yan, Y., Wang, J. (2011). Effect of B2O3 on Melting Temperature, Viscosity and Desulfurization Capacity of CaO–based Refining Flux. *ISIJ International*, 51 (5), 702–706.

[88] Wu, G., Yazhenskikh, E., Hack, K., Wosch, E., Müller, M. (2015). Viscosity model for Oxide Melts Relevant to Fuel Slags. Part 1: Pure Oxides and Binary Systems in The System SiO2–Al2O3–CaO–MgO–Na2O–K2O. *Fuel Processing Technology*, 137, 93–103.

[89] Carter, C.B and Norton, M.G. (2007). *Ceramic Materials - Science and Engineering*. New York: Springer Science+Business Media.

[90] Mintova, S., Jaberbc, M., Valtcheva, M. (2015). Nanosized microporous crystals: emerging applications. *Chem Soc Rev,* 44, 7207-7233.

[91] Dermiencea, M., Lognaya, G., Mathieub, F., Goyens, P. (2014). Effects of thirty elements on bone metabolism. *Journal of Trace Elements in Medicine and Biology*, 32, 86-106.

[92] Pizzorno, L. (2015). Nothing boring about boron. *Integrative Medicine*, 14 (4), 35-48.

[93] Ali, A.A., Baumli, P. and Mucsi, G. (2001). Mechanical Alloying and Milling. Hungaria: University of Miskolc.

[94] King, A.G. (2002). In Chapter 3: Milling and Equipment. *Ceramic Technology and Processing* (p. 20–55). New York: William Andrew-Noyes Publications.

[95] Lu, S.Y., Mao, Q.J., Peng, Z., Li, X.D., Yan, J.H. (2012). Simulation of ball motion and energy transfer in a planetary ball mill. *Chinese Physics B*, 21 (7), 1–9.

[96] El-Eskandarany, M.S. (2015). In Chapter 3: Controlling the powder milling process. *Mechanical Alloying: Nanotechnology, Materials Science and Powder Metallurgy* (p. 48-83). MA, USA: William Andrew Pub.

[97] Taygun, M.E. and Boccaccini, A.R. (2018). Chapter 10: Nanoscaled bioactive glass particles and nanofibers. Ylanen, H. (Editor), in *Bioactive glasses: Materials, Properties and Applications* (p. 235-284). Duxford: Woodhead Publishing.

[98] Martinez-Pastor, F., Johannisson, A., Gil, J., Kaabi, M., Anel, L., Paz, P., Rodriguez-Martinez, H. (2004). Use of chromatin stability assay, mitochondrial stain JC-1, and fluorometric assessment of plasma membrane to evaluate frozen-thawed ram semen. *Animal Reproduction Science*, 84 (1–2), 121–133.